European Journal of Medicinal Chemistry 294 (2025) 117732

Contents lists available at ScienceDirect

European Journal of Medicinal Chemistry

journal homepage: www.elsevier.com/locate/ejmech

Research paper

Identification of isoxazole-based TRPA1 inhibitors with analgesic effects in vivo

Valentina Albanese [a,1,3], Matilde Marini [b,1], Martina Tesi [b], Lorenzo Landini [b], Elisa Bellantoni [b], Sandro Cosconati [c], Michele Roggia [c], Lorenzo Tagliazucchi [d], Lorenzo Gnudi [e], Valentina Puscio [e], Chiara Sturaro [f], Chiara Ruzza [f], Remo Guerrini [e,g], Pierangelo Geppetti [b], Romina Nassini [b,*], Delia Preti [e,**], Francesco De Logu [b,2], Salvatore Pacifico [e,2]

[a] Department of Environmental and Prevention Sciences, University of Ferrara, Palazzo Turchi di Bagno, C.so Ercole I D'Este 32, 44121, Ferrara, Italy
[b] Department of Health Sciences, Clinical Pharmacology and Oncology Section, Viale Pieraccini 6, University of Florence, Florence, 50139, Italy
[c] DiSTABiF, Università della Campania Luigi Vanvitelli, Via Vivaldi 43, Caserta, 81100, Italy
[d] Department of Life Sciences, University of Modena and Reggio Emilia, Via Campi 103, 41125, Modena, Italy
[e] Department of Chemical, Pharmaceutical and Agricultural Sciences, University of Ferrara, Via Luigi Borsari 46, 44121, Ferrara, Italy
[f] Department of Neuroscience and Rehabilitation, University of Ferrara, Via Luigi Borsari 46, Ferrara, 44121, Italy
[g] Technopole of Ferrara, Laboratory for Advanced Therapies (LTTA), via Fossato di Mortara 70, 44121, Ferrara, Italy

ARTICLE INFO

Keywords:
TRPA1 receptor
TRPA1 inhibitors
Pain signalling
Isoxazole derivatives

ABSTRACT

The transient receptor potential ankyrin 1 (TRPA1) channel has been extensively studied as a potential therapeutic target for the treatment of different pain types, with better efficacy and safety profiles compared to current therapies. Because TRPA1 is implicated in different pathophysiological processes, selective antagonists of this channel could provide therapeutic benefits beyond pain relief. In this study, we report the design and synthesis of a novel series of carboxamide derivatives incorporating an isoxazole moiety, which were evaluated for their ability to inhibit TRPA1-mediated signalling. Among these, we identified the TRPA1 antagonists **12** and **13** displaying nanomolar potency *in vitro* and significant analgesic effects against the TRPA1 agonist, allyl isothiocyanate and in the formalin test in mice. Docking analyses were also conducted to explore the binding modes of the most representative compounds with the proposed pharmacological target.

1. Introduction

The transient receptor potential ankyrin 1 (TRPA1) channel is a non-selective cation channel that plays a crucial role in nociception, thermosensation, and various physiological processes [1]. Structurally, it consists of four identical subunits, each containing six hydrophobic transmembrane domains, which together form a homotetramer surrounding the central pore [2]. The channel is named for its distinctive N-terminal region containing 14 to 18 ankyrin repeats, which are critical for mediating interactions with other proteins as well as for channel insertion and regulation in the plasma membrane. As a member of the broader TRP family of ion channels, TRPA1 is primarily expressed in sensory neurons where is particularly known for its role in the perception of pain [3,4]. Activation of TRPA1 channels results in the influx of sodium and calcium ions, causing depolarization of the nociceptive nerve endings, which are implicated centrally to the propagation of the pain signals and peripherally in the release of sensory neuropeptides, mainly calcitonin gene related peptide (CGRP), to elicit neurogenic inflammation [5]. The recent localization of TRPA1 in Schwann cells, that surround peripheral nerve terminals, revealed the channel role via release of reactive oxygen species (ROS) in sustaining neuropathic [6], cancer [7,8] and migraine pain [9].

The TRPA1 channel is activated by a heterogeneous array of endogenous and exogenous stimuli [10], including allyl isothiocyanate

* Corresponding author.
** Corresponding author.
E-mail addresses: romina.nassini@unifi.it (R. Nassini), prtdle@unife.it (D. Preti).
[1] These authors equally contributed to the work.
[2] F.D.L and S.P. shared senior co-last position.
[3] V.A.: Department of Chemical, Pharmaceutical and Agricultural Sciences, University of Ferrara, Via Luigi Borsari 46, 44,121 Ferrara, Italy.

https://doi.org/10.1016/j.ejmech.2025.117732
Received 20 February 2025; Received in revised form 28 April 2025; Accepted 6 May 2025
Available online 9 May 2025
0223-5234/© 2025 The Authors. Published by Elsevier Masson SAS. This is an open access article under the CC BY license (http://creativecommons.org/licenses/by/4.0/).

(AITC, mustard oil), acrolein, and various electrophilic thiol-reactive agonists which can induce pain and inflammation by covalently modifying the cysteine and lysine residues at the N-terminal of the receptor. Channel activators encompass non-electrophilic agonists that interact with TRPA1 through non-covalent interactions [11–13].

Given its prominent role in pain signalling pathways, TRPA1 has garnered significant interest as a therapeutic target for the development of novel analgesics [14–16]. TRPA1 antagonists have been shown to effectively reduce pain responses in various preclinical models, highlighting their potential utility in treating pain conditions. Additional roles of TRPA1 in non-painful conditions such as regulation of airway hyperreactivity [17], ocular diseases [18], neurodegenerative diseases [19] and cardiovascular function [20], suggests and expand the therapeutic potential of channel antagonists [1,16].

This promising potential of TRPA1 as a suitable drug target has faced several challenges. Early attempts to produce TRPA1 antagonists resulted in compounds that, while effective in preclinical models, exhibited limited efficacy or off-target side effects in clinical trials complicating their therapeutic use [14,16]. Improvement in the early identification and optimization of new TRPA1 antagonists [16] has taken advantage by several novel strategies, including cryo-electron microscopy structure studies [2,17,21].

Here, we outlined the design and synthesis of a new series of carboxamide derivatives featuring an isoxazole moiety that have been investigated for the capability to inhibit TRPA1-mediated signalling. Among them, we identified potent TRPA1 antagonists *in vitro*, which also demonstrated significant analgesic effects in mouse pain models. Furthermore, docking analyses were performed to investigate the binding mode of the most representative compounds with respect to the proposed pharmacological target.

2. Results and discussion

2.1. Design and synthesis of novel TRPA1 antagonists

To identify novel TRPA1 receptor antagonists, we used compounds with general structure **1** (Fig. 1) as our starting point, drawing inspiration from previous patent literature [22]. The reference scaffold **1** consists of a proline sulfonamide moiety connected via an amide bond to a hexatomic heterocyclic core. This core was substituted with a phenyl ring bearing at the para position groups with different steric and electronic properties. The structural analysis of compound GDC-0334 (PDB 6WJ5) [17], a member of this family, bound to TRPA1 revealed that the proline sulfonamide portion forms multiple interactions with a single TRPA1 subunit, including contacts with the S5 and S6 helices, pore helix 1, and the S4–S5 linker. Conversely, the biaryl moiety, forming a lipophilic tail, would play a limited role in receptor interactions. However, its lipophilicity is crucial for membrane partitioning and access to the binding site.

With the aim of expanding the structure-activity relationship (SAR) information about this class of antagonists and in the search for even more potent and promising compounds, we decided to synthesize two series of derivatives in which the reference template 1 was sequentially modified in the two key regions mentioned above (shown in blue and red in Fig. 1).

In the first series (compounds **10**–**19**, see the structures in Table 1), we investigated the effect of modifying the lipophilic tail of the reference template **1** (blue in Fig. 1) by replacing the six-member heterocycle with an isoxazole nucleus. This structural modification, to our knowledge, has not been previously investigated in this class of TRPA1 antagonists. The isoxazole ring was differently functionalized at the 5- and/or at the 4-position: at the 5-position we introduced a phenyl ring bearing few *p*-subsitutions (R in Fig. 1) that were mostly suggested by previous SAR studies on **1** [22]; the 4-position of the isoxazole was substituted with halogens, aryl groups, or phenylethynyl moieties primarily with the aim to investigate the steric effects in this region of the molecules and, to some extent, to increase their lipophilicity, thereby enhancing their interaction with the lipid bilayer.

In the second generation of compounds, we examined the effects of replacing the proline core (red in Fig. 1) with thiazolidine (**22a**), six-membered heterocycles (**22b-d**, **24**–**25**), and fused heterocycles (**22e-g**). These substitutions, combined with the most effective modifications from the first series, were explored with the aim to enhance the interaction of the new antagonists with the target protein's binding site.

The first series of compounds was synthesized as shown in Scheme 1. Starting from commercially available acetophenones (**2a-c**), the corresponding ethyl 5-phenylisoxazole-3-carboxylates (**3a-c**) were obtained through a two-step reaction with ethyl oxalate followed by treatment with hydroxylamine. The resulting esters were then reduced with $LiAlH_4$ to the corresponding alcohols (**4a-c**), which were subsequently converted into the alkyl halide derivatives (**5a-c**) via the Appel reaction. The Gabriel reaction was applied to convert the brominated analogues into amine derivatives (**7a-c**), which were amidated with different sulfonyl-L-proline derivatives (**9d-e**) to yield the desired first series of antagonists (**10**–**13**). The proline residues were prepared by reacting an appropriate sulfonyl chloride (**8d** or **8e**) with a proteinogenic proline residue.

Iodination of compounds **12** and **13** using *N*-iodosuccinimide in trifluoroacetic acid afforded the intermediates **14** and **15**. Subsequent Suzuki cross-coupling reactions with appropriate boronic acids yielded compounds **16**–**18**, while Sonogashira coupling with phenylacetylene led to compound **19**.

The second series of compounds was obtained as depicted in Scheme 2. The chemical approach began with the *N*-sulfonylation of different amino acids (**20a-g**, **23**) using 4-fluorobenzenesulfonyl chloride to yield the respective sulfonamides (**21a-g**, **24**). The resulting carboxylic acid derivatives were coupled with **7c** to produce compounds **22a-g** and **25**. Compound **25** was further treated with trifluoroacetic acid to remove the Boc protection, yielding the piperazine derivative **26**.

All the final compounds were shown to have a purity higher than 95 % following HPLC analysis (HPLC traces have been provided in the SI).

2.2. Inhibition of TRPA1 opening in vitro

The synthesized isoxazole derivatives were initially tested for their ability to inhibit the calcium (Ca^{2+}) response evoked by the TRPA1 agonist benzyl isothiocyanate (BITC, 10 μM) at a concentration of 1 μM in A549 cells expressing the native human channel (Table 1 and Fig. 2) [23]. In this assay, compounds **11**, **12**, **13**, **17**, were found to reduce more than 60 % of the BITC-mediated Ca^{2+} response and their IC_{50} were determined in both A549 (Table 1 and Fig. 2) and hTRPA1-HEK293 cells stably transfected with human TRPA1 (Table 2 and Fig. 3). The TRPA1

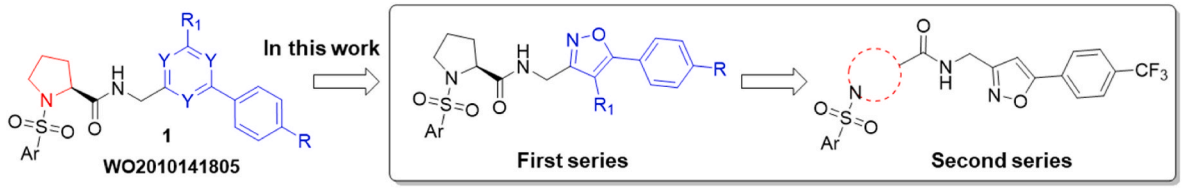

Fig. 1. Rational design of the newly synthesized compounds.

Table 1
In vitro evaluation of the investigated compounds as TRPA1 antagonists in A549 cells.

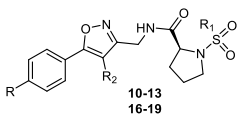

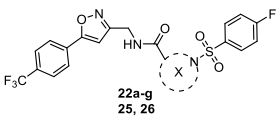

Compound[a]	R	R_1	R_2	X	Inhibitory rates of hTRPA1 (%)[b]	IC_{50}[c] (nM)
A967079					61.73 ± 1.24	41 (CI: 31–54)
10	H	4-F-Ph	H	–	34.74 ± 3.69	–
11	Cl	4-F-Ph	H	–	67.73 ± 2.02	165 (CI: 101–264)
12	CF_3	4-F-Ph	H	–	70.28 ± 1.88	45 (CI: 29–73)
13	CF_3	5-Cl-thiophene	H	–	75.16 ± 1.21	49 (CI: 35–67)
14	CF_3	4-F-Ph	I	–	27.08 ± 3.30	–
16	CF_3	4-F-Ph	Ph	–	35.62 ± 4.32	–
17	CF_3	4-F-Ph	4-CF_3-Ph	–	77.41 ± 2.35	494 (CI: 315–747)
18	CF_3	5-Cl-thiophene	4-CF_3-Ph	–	35.70 ± 3.56	–
19	CF_3	4-F-Ph	—≡—Ph	–	44.57 ± 4.18	–
22a	–	–	–		39.64 ± 2.45	–
22b	–	–	–		1.28 ± 5	–
22c	–	–	–		38.78 ± 4.32	–
22d	–	–	–		21.12 ± 4.84	–
22e	–	–	–		48.60 ± 2.73	–
22f	–	–	–		32.12 ± 4.19	–
22g	–	–	–	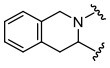	6.85 ± 4.97	–
25	–	–	–	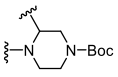	41.30 ± 3.40	–
26	–	–	–		12.90 ± 4.14	–

[a] Compounds were tested at 1 μM dose.
[b] % of inhibition *vs* BITC (10 μM) *in vitro*.
[c] Measured for compounds with a % inhibition >60 % *in vitro*.

selective antagonist A967079, which produced the 61.73 ± 1.24 % and 90.44 ± 1.87 % inhibition of the Ca^{2+} response induced by BITC (10 μM) in A549 and hTRPA1-HEK293 cells, respectively, was used as reference compound. Its potency was confirmed by IC_{50} values of 41 nM (CI: 31–54 nM) in A549 cells and 58 nM (CI: 43–77 nM) in hTRPA1-HEK293 cells [24].

As stated above, the selection of substitution patterns in our derivatives was partially driven by previous SAR studies on related TRPA1 antagonists [22]. In the first series of compounds, a 4-(fluorophenyl) sulfonyl group enhanced activity only when combined with electron-withdrawing groups (Cl or CF_3) on the phenyl ring linked to the isoxazole (compare compounds **10**–**12**).

Considering the higher potency of **12** (A549 cells: IC_{50} = 45 nM; hTRPA1-HEK293 cells: $IC_{50:}$ 65 nM) compared to compound **11** (A549 cells: IC_{50} = 170 nM; hTRPA1-HEK293 cells: $IC_{50:}$ 128 nM) and recognizing that organofluorine compounds can exhibit more favourable drug-like properties [25], the CF_3 substitution was retained as R moiety in most cases. The replacement of the 4-F-Ph framework of **12** with a 5-Cl-thiophene ring (compound **13**) had a minimal impact on potency in both cell lines.

In contrast, substituting the 4-position of the isoxazole with iodine (**14**), aryl (compounds **16**–**18**) or phenylethynyl (compound **19**) moieties was found to be mostly detrimental to activity except for compound **17** which displayed a % of inhibition higher than that of A967079 in both A549 and hTRPA1-HEK293 cells. Nevertheless, the potency of this compound in terms of IC_{50} was significantly lower than that of the internal reference especially in A549 cells.

We then explored the potential effects of replacing the proline

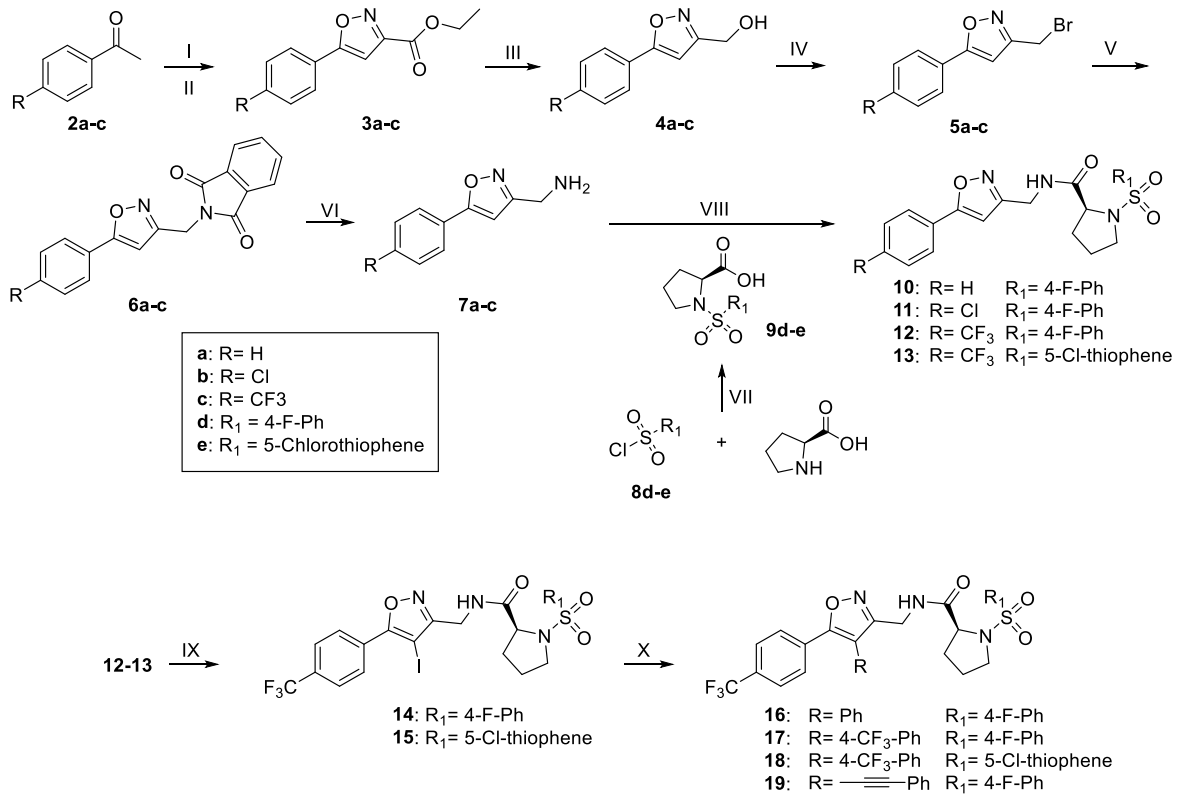

Scheme 1. Synthetic pathway for the preparation of the first series of compounds (**10**–**13**, **16**–**19**). Reagents and conditions: I) Ethyl oxalate, EtONa, 50 °C to reflux, absolute EtOH, 2h; II) NH_2OH, reflux, absolute EtOH, 5h; III) $LiAlH_4$, 0 °C to rt, THF, 3h; IV) CBr_4,PPh_3, 0 °C to rt, dry THF, 12h; V) Phthalimide, NaH, reflux, CH_3CN, 4h; VI) $NH_2NH_2xH_2O$, reflux, EtOH, 1h; VII) $NaHCO_3$, 50 °C, H_2O, 16h; VIII) HATU, DIPEA, 0 °C to rt, DMF, 4h; IX) *N*-iodosuccinimide, rt, TFA, 30 min; X) for compounds **16**–**18**: appropriate phenylboronic acid, K_2CO_3, $Pd(PPh_3)_4$, 80 °C, toluene/EtOH/H_2O (2:1:1.5), 16 h; for compound **19**: phenylacetylene, Et_3N, CuI, $PdCl_2(PPh_3)_2$, 50 °C, THF, 12 h.

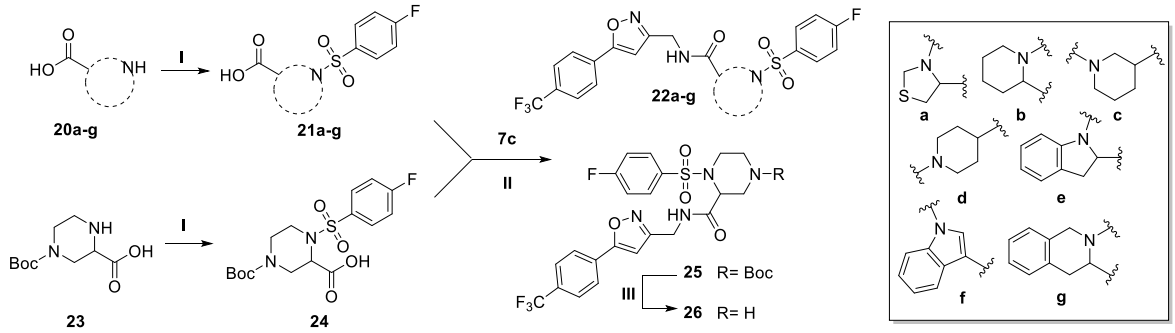

Scheme 2. Synthetic pathway for the preparation of the second series of compounds (**22a-g**, **25**–**26**). Reagents e conditions: I) 4-Fluorobenzenesulfonyl chloride, $NaHCO_3$, 50 °C, H_2O, 16h; II) HATU, DIPEA, 0 °C to rt, DMF, 4h; III) TFA, rt, 30 min.

residue with alternative non-natural cyclic amino acid-like spacers (compounds **22a-g**, **25**, **26**). However, the presence of a pyrrolidine linker appeared to be essential for maintaining antagonist potency. Notably, we observed a significant retention of activity only with the indole derivative **22e**.

Collectively, these findings confirmed the feasibility of replacing the hexaatomic core with a 5-membered heterocycle in TRPA1 antagonists with general structure **1** (Fig. 1), while preserving activity. Conversely, increasing steric hindrance at the 4-position of the isoxazole ring or modifying the proline framework was detrimental to activity. An overview of the results from the SAR analysis has been provided in Fig. 4. Of the investigated derivatives, compounds **12** and **13** exhibited potency comparable to that of A967079 in A549 and hTRPA1-HEK293 cells, a highly potent antagonist tool within this research field. Given their promising *in vitro* profile, these compounds were selected for evaluation of their ability to inhibit TRPA1 opening *in vivo*.

2.3. Molecular modeling

To shed lights into the binding properties of the novel discovered TRPA1 receptor antagonists, in silico studies were undertaken. Specifically, docking experiments were attained employing the CryoEM structure of TRPA1 receptor (PDB ID: 6WJ5) [17] in complex with its antagonist GDC-0334. Here, AD4-GPU docking software was employed to predict the binding conformation of **12** within the TRPA1 protein [26]. The choice to include **12** in this investigation was based on its *in vitro* antagonist activity (Table 1). As expected, the predicted binding mode of **12** closely resemble that of the experimentally determined

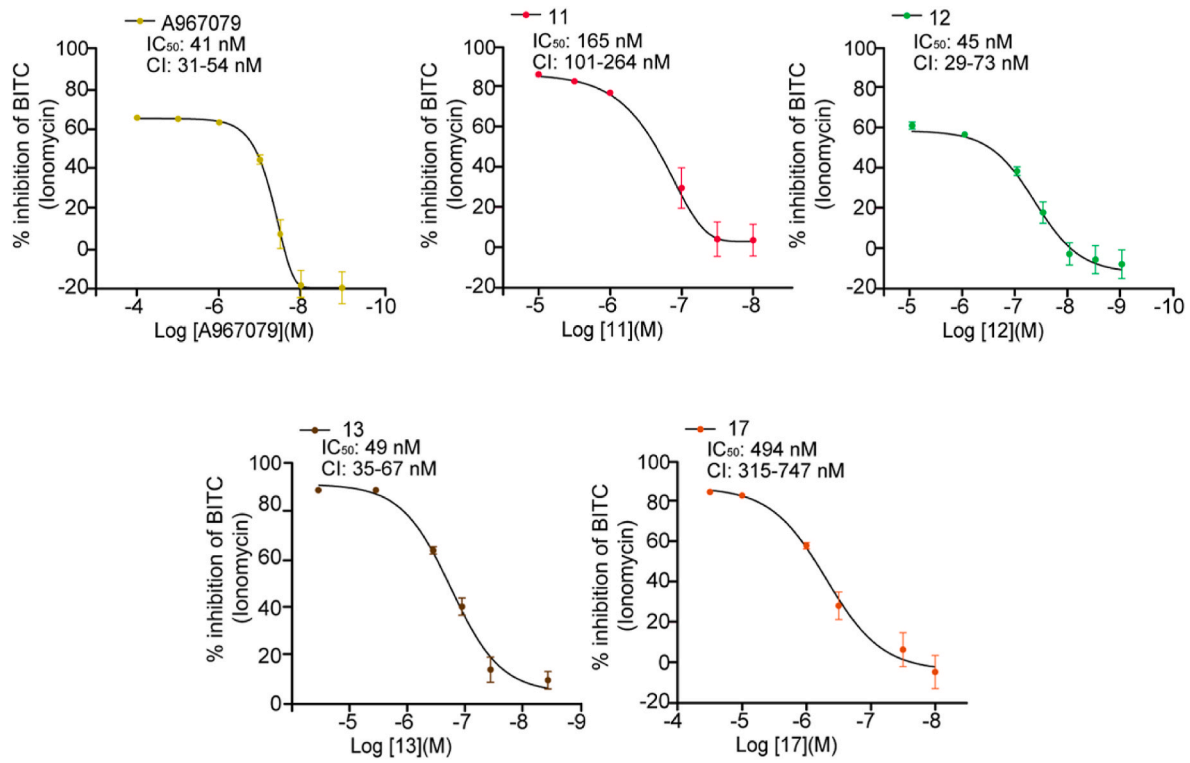

Fig. 2. ***In vitro*** **evaluation of isoxazole derivatives to inhibit the TRPA1-dependent calcium response in A549 cells.** Half-maximal inhibitory concentration (IC_{50}) and confident interval (CI) values of A96 (cells number: 100 μM = 203, 10 μM = 301, 1 μM = 195, 100 nM = 228, 30 nM = 88, 10 nM = 99, 1 nM = 119), **11** (cells number: 10 μM = 171, 3 μM = 388, 1 μM = 285, 100 nM = 43, 30 nM = 94, 10 nM = 112), **12** (cells number: 10 μM = 168, 1 μM = 449, 100 nM = 113, 30 nM = 102, 10 nM = 232, 3 nM = 109, 1 nM = 105), **13** (cells number: 10 μM = 162, 1 μM = 124, 100 nM = 306, 30 nM = 236, 10 nM = 243, 1 nM = 218) and **17** (cells number: 30 μM = 147, 10 μM = 136, 1 μM = 301, 300 nM = 124, 30 nM = 114, 10 nM = 158). Mean ± sem.

Table 2
In vitro evaluation of the investigated compounds as TRPA1 antagonists hTRPA1-HEK293 cells.

Compound[a]	Inhibitory rates of hTRPA1 (%)[b]	IC_{50} (nM)
A967079	90.44 ± 1.87	58 (CI: 43–77)
11	92.92 ± 0.35	128 (CI: 92–180)
12	96.12 ± 0.57	65 (CI: 54–78)
13	93.25 ± 0.43	67 (CI: 51–88)
17	92.79 ± 0.63	99 (CI: 78–127)

[a] Compounds were tested at 1 μM dose.
[b] % of inhibition *vs* BITC (10 μM) *in vitro*.

(Fig. 5a) GDC-0334 ligand. In particular, the proline sulfonamide moiety and the *p*-substituted phenyl ring of both structures are strongly overlapped, both establishing proficient hydrophobic interactions with the nearby amino acid L870 side chain on S4–S5 linker, I878 and L881 side chains on S5 helix, F944, and L952 and L956 side chains on S6 helix. In this position, the isoxazole nucleus and the attached CF3 *p*-substituted phenyl of **12** form extended π-π interactions with the nearby F909 side chain on Pore helix 1 (Fig. 5b). It has been demonstrated in previous papers that residue F909 is crucial for the antagonist activity [27,28], thus it is tempting to postulate that the comparable activity obtained for **12** with respect to A967079 (Table 1) is ascribable to the presence of the above described π-stacking interactions with F909 side chain, coupled with van der Waals interactions made with the hydrophobic residues within the pocket where **12** is predicted to be nestled. As expected, the bioisosteric substitution (phenyl of **12** with thienyl of **13**, Table 1) in R_1 does not affect the antagonist activity, thereby postulating that **12** and **13** might have a similar binding pose within the TRPA1 protein.

For the first series of compounds, we infer that the electron-withdrawing substitution on the phenyl ring (such as CF_3 of **12**) diminishes the electron density of the π-cloud, allowing for a stronger π-stacking interaction [29]. To further understand the effect of substitution on the *p*-substituted phenyl ring, the electrostatic potentials (ESPs) mapped onto electron density isosurfaces were calculated for **11** and **12** using the Jaguar program [30] within the Maestro suite developed by Schrodinger (Fig. 6, Schrödinger Release 2024–4: Maestro, Schrödinger, LLC, New York, NY, 2024). As highlighted by this analysis, the CF_3 substitution of **12** (Fig. 6b), leads to more positive ESPs values of the phenyl group, enhancing its capability of interacting with the F909 side chain through π-π interactions.

Additionally, among all the substitutions explored for the first series, it appears evident that the substitution at position 4 of the isoxazole ring (**14**–**19** R2 Table 1) is detrimental for the activity probably due to the augmented steric hindrance given by these groups that do not allow the correct orientation of the adjacent *p*-substituted phenyl ring, preventing its correct parallel orientation towards the F909 side chain.

Concerning the second series (**22a-g**, **25**–**26** Table 1), the substitution of the $_L$-proline with other conformationally constrained and bulkier groups is detrimental for the TRPA1 antagonist activity due to the limited extension of the hydrophobic pocket where the $_L$-proline of **12** is lodged.

2.4. *In vivo inhibitory response in mouse model of pain*

Based on their potency to inhibit the TRPA1 channel, which is comparable to the reference compound A967079, compounds **12** and **13** were also evaluated in *in vivo* tests. The ability of intraplantar (i.pl.) administration of compounds **12** and **13** to inhibit the nociceptive response evoked by i.pl. injection of AITC (10 nmol/10 μl) was assessed in C57BL/6J mice. Both compounds reduced the AITC evoked nociceptive response in a dose-dependent (1–300 nmol/10 μl, i.pl.) manner with ID_{50} of 6.5 nmol, (CI: 2.7–14.5 nmol) for compound **12**, 11.5 nmol

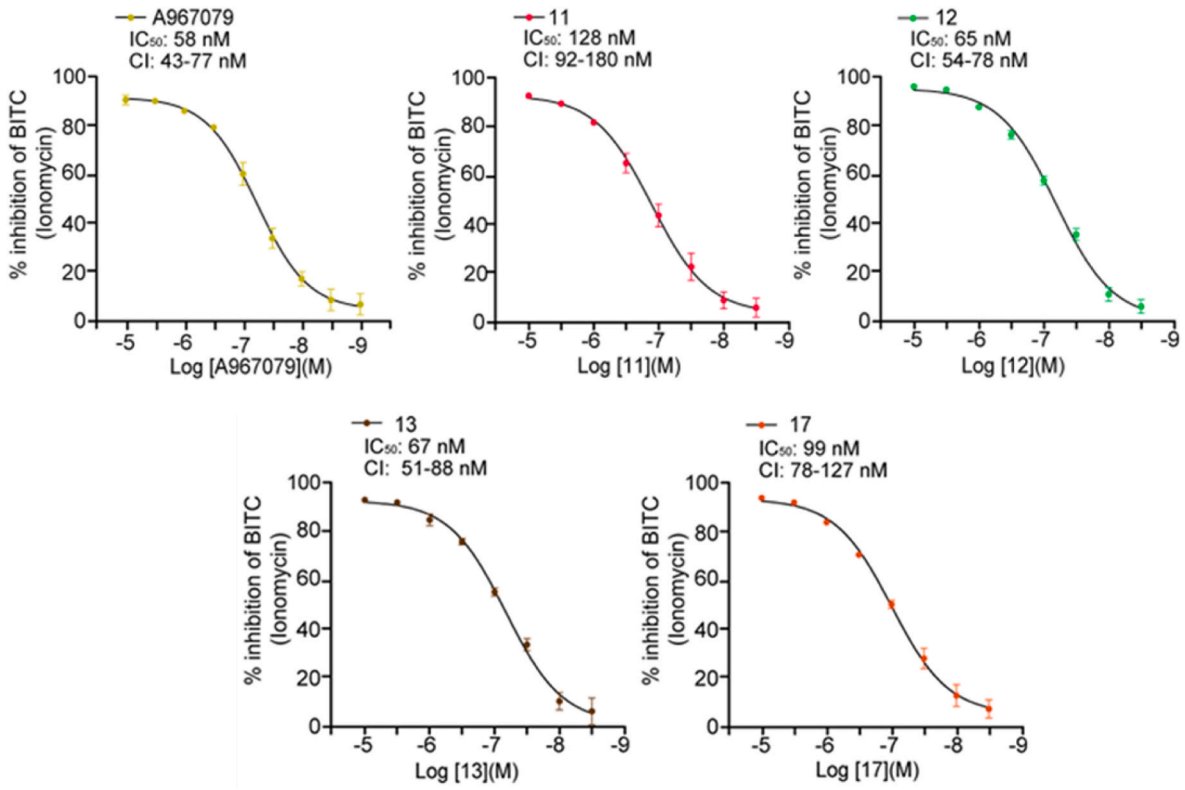

Fig. 3. ***In vitro*** **evaluation of compounds 11,12,13 and 17 to inhibit the TRPA1-dependent calcium response in hTRPA1-HEK293 cells.** Half-maximal inhibitory concentration (IC_{50}) and confident interval (CI) values of A96 (cells number: 10 μM = 79, 3 μM = 91, 1 μM = 111, 300 nM = 103, 100 nM = 107, 30 nM = 72, 10 nM = 92, 3 nM = 110, 1 nM = 98), **11** (cells number: 10 μM = 124, 3 μM = 134, 1 μM = 126, 300 nM = 84, 100 nM = 119, 30 nM = 106, 10 nM = 151, 3 nM = 115), **12** (cells number: 10 μM = 132, 3 μM = 92, 1 μM = 97, 300 nM = 90, 100 nM = 102, 30 nM = 110, 10 nM = 112, 3 nM = 91), **13** (cells number: 10 μM = 128, 3 μM = 114, 1 μM = 105, 300 nM = 117, 100 nM = 107, 30 nM = 101, 10 nM = 97, 3 nM = 116) and **17** (cells number: 10 μM = 112, 3 μM = 63, 1 μM = 129, 300 = 97, 100 nM = 126, 30 nM = 96, 10 nM = 78, 3 nM = 102). Mean ± sem.

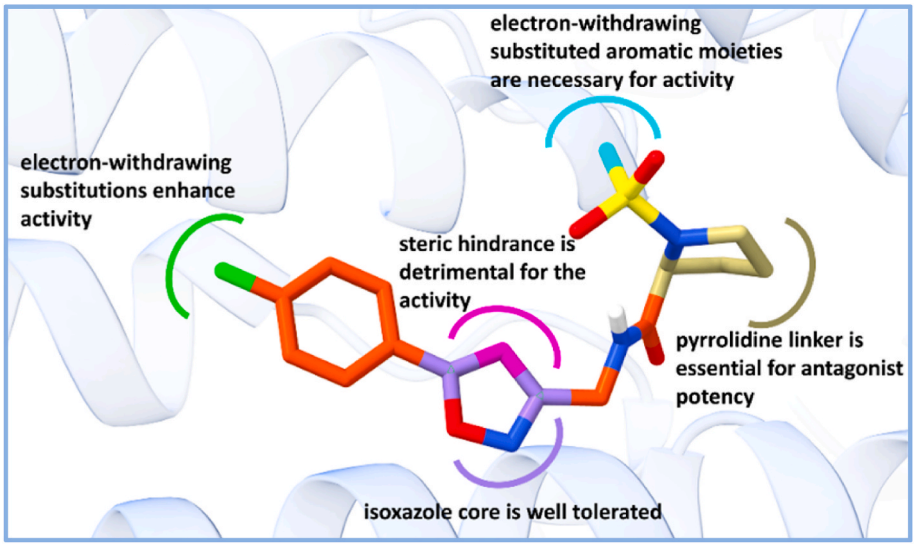

Fig. 4. Summary of the SAR analysis for the compounds investigated in the *in vitro* assays.

(CI:6.4–20.9 nmol) for compound **13,** and 21.3 nmol (CI:10.7–42.2 nmol) for the reference compound, A967079 (Fig. 7a).

Pharmacologic blockade or genetic ablation of TRPA1 have been previously shown to attenuate the flinching, licking and lifting responses of phase I and II caused by the intraplantar injection of formalin [31]. Compounds **12** and **13** (both intraplantar, 50 nmol/10 μl), tested in the formalin test (0.5 %/20 μl, i.pl.), reduced the licking and lifting responses similarly to the reference compound (A967079, Fig. 7b).

3. Conclusions

Although the TRPA1 channel represents a promising target for the development of novel analgesics, recent clinical findings underline the limited efficacy of currently investigated antagonists [32,33]. After the

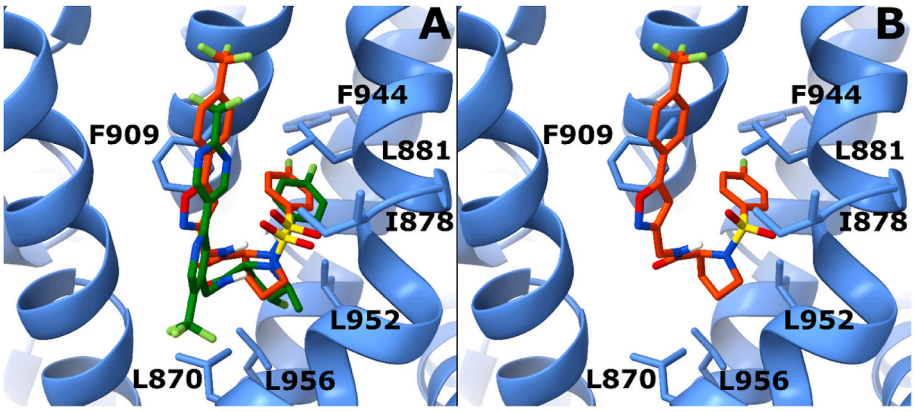

Fig. 5. (A) Overlap between co-crystal ligand GDC-0334 and predicted binding mode of 12, represented as green and orange sticks. The TRPA1 protein structure is represented as blue sticks and ribbons. (b) Predicted binding mode of **12** in complex with TRP.

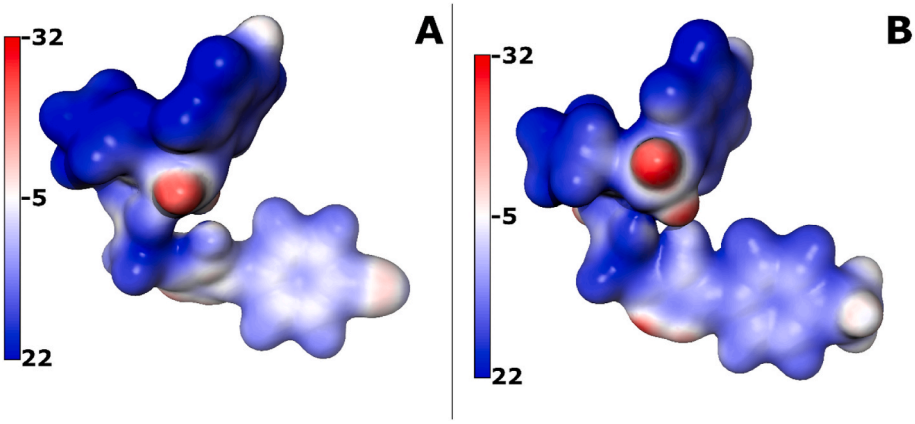

Fig. 6. ESPs mapped onto electron density isosurfaces (ρ = 0.0002) for **11** (a) and **12** (b).

poor selectivity of early clinical candidates, recent advancements in drug design drive the discovery of TRPA1 antagonists with promising therapeutic potential. In this work we report compounds **12** and **13** which exhibit a high potency *in vitro* and e efficacy in alleviating pain-like responses *in vivo*. Given the prominent role of TRPA1 in pain signalling the two molecules may warrant future development and further optimization to improve pharmacodynamic and pharmacokinetic features and testing in pathophysiological pain models of pain and in non-painful conditions with translational value for human diseases.

4. Experimental section

4.1. Chemistry

4.1.1. Materials and methods

Reagents were supplied by BLD, Sigma-Aldrich, and Fluorochem. Reaction progress was monitored by thin-layer chromatography (TLC) on precoated F_{254} Macherey-Nagel silica gel plates (UV lamp at 254 nm) and/or by electrospray mass spectrometry using an ESI MICROMASS ZMD 2000. Crude products were purified by column chromatography or via semipreparative reverse-phase HPLC using a Waters 600 Multisolvent Delivery System, equipped with a Jupiter C18 column (250 × 30 mm^2, 300 Å, 15 μm spherical particle size) and a UV detector set at 220 nm. The column was perfused at a flow rate of 20 mL/min with a linear gradient, programmed as needed, of solvent A (100 % H_2O and 0.1 % v/v TFA) and solvent B (40 % H_2O, 60 % CH_3CN, and 0.1 % v/v TFA). Analytical RP-HPLC analyses were performed on a HPLC–UV apparatus (Agilent 1200 Series, Germany). The analytical purity of the final compounds was assessed using a Phenomenex Kinetex C18 column (150 × 4.6 mm, 5 μm particle size) and a variable wavelength UV detector set at 220 nm. All final compounds were >95 % pure by HPLC analysis (see the Supporting Information). Analyses were conducted with an eluent consisting of H_2O and CH_3CN, both containing 0.1 % v/v TFA, at a flow rate of 0.5 mL/min, using a gradient from 0 to 100 % CH_3CN over 25 min. Retention times (T_R) of the final compounds from analytical HPLC are reported in minutes. ^1H NMR and ^{13}C NMR spectra were recorded at room temperature on a Varian 400 MHz spectrometer. The signals were referenced to the residual ^1H shift of the deuterated solvents (δ H 7.26 for $CDCl_3$; δ H 2.50 for DMSO-d_6). Chemical shifts (δ) are expressed in parts per million (ppm), using the peak of tetramethylsilane as an internal standard in deuterated solvents, while coupling constants (J) are reported in Hertz (Hz). Splitting patterns are designated as s, singlet; d, doublet; t, triplet; q, quartet; m, multiplet; and b, broad. High-resolution mass spectra were obtained using an UltiMate 3000 UHPLC (Thermo Fisher) coupled to an Orbitrap Q-Exactive Hybrid HRMS (see the SI for further details).

4.1.2. General procedure for the synthesis of isoxazole esters ***3a-c***

To a freshly prepared suspension of Na (489 mg) in absolute EtOH (40 mL), a solution containing the appropriate acetophenone **2a-c** (10.64 mmol) and ethyl oxalate (21.27 mmol) in absolute EtOH (10 mL) was added dropwise at 50 °C. The resulting mixture was then refluxed for 2 h under stirring. Upon completion of the reaction, the solvent was removed under reduced pressure and the mixture treated with 1 M HCl until acidic, followed by stirring at room temperature for 1 h. The mixture was subsequently extracted with AcOEt (2x40 mL). The

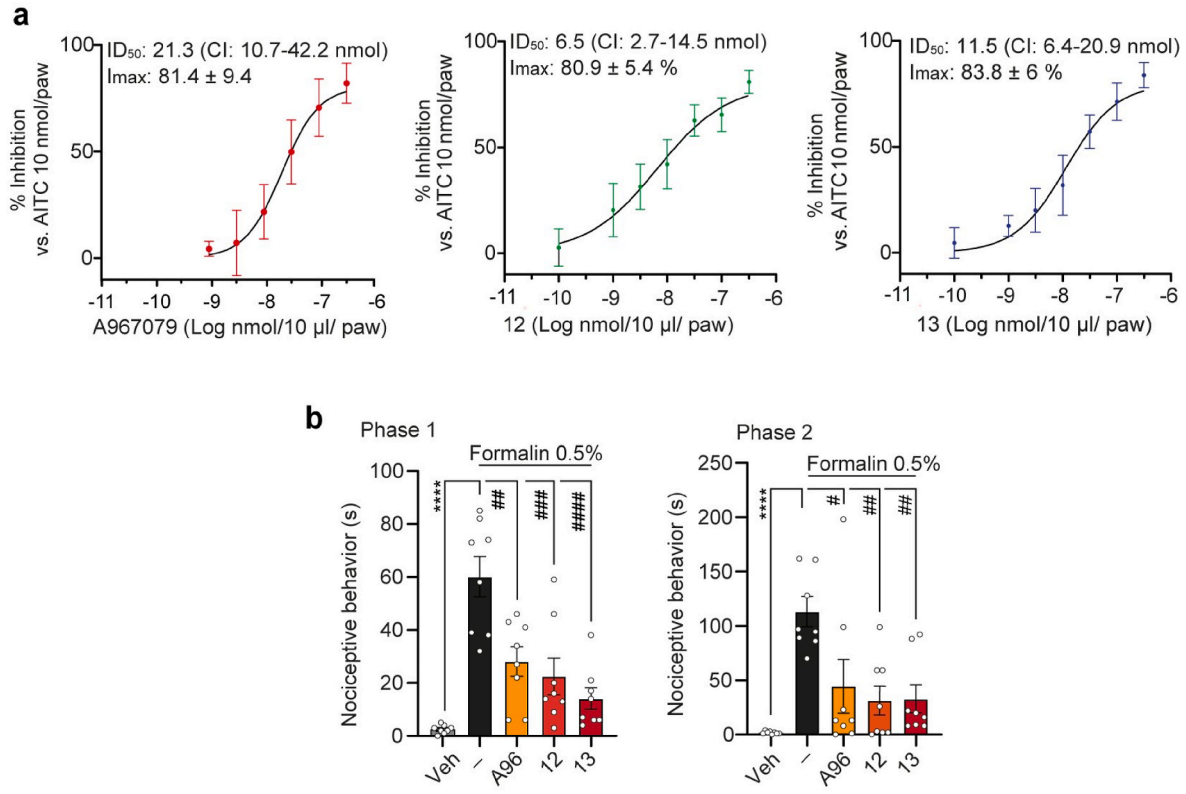

Fig. 7. ***In vivo*** **evaluation of compound 12 and 13 to inhibit TRPA1-dependent nocifensive behaviors in mice. a** Dose response curve and ID_{50} values for the inhibition (%) of the nociceptive response induced by AITC (10 nmol/10 µl, intraplantar, i.pl.) by A967079 and compounds **12** and **13** in C57BL/6J mice. **b** Compounds **12** and **13** and A967079 (50 nmol/10 µl, i.pl.) significantly reduce both phase I and phase II of the nociceptive response to formalin (0.5 %/20 µl, i.pl.) in C57BL/6J mice (n = 8 mice per group). Mean ± sem. ***p < 0.001, ****p < 0.0001 $^{\#}$p < 0.05 $^{\#\#}$p < 0.01, $^{\#\#\#}$p < 0.001, $^{\#\#\#\#}$p < 0.0001 one-way ANOVA and Bonferroni post hoc test.

combined organic phases were washed with water and brine, and after drying over Na_2SO_4, the solvent was evaporated. The resulting semisolid residue was dissolved in absolute EtOH, followed by the addition of hydroxylamine hydrochloride (10.64 mmol) at rt. The mixture was refluxed for 5 h, followed by extraction with AcOEt and H_2O. The crude product was triturated using petroleum ether, yielding the desired compound as a crystalline solid.

4.1.3. Ethyl 5-phenylisoxazole-3-carboxylate ***(3a)***

White crystalline solid (55 % yield). ^{1}H NMR (400 MHz, DMSO-d_6): δ 7.97–7.94 (m, 2H), 7.59–7.51 (m, 3H), 7.50 (s, 1H), 4.4 (q, J = 7.2, 2H), 1.34 (t, J = 6.8, 3H). MS (ESI): *m/z* calcd for $C_{12}H_{11}NO_3$ $[M+H]^+$ 218.23; found, 218.26.

4.1.4. Ethyl 5-(4-chlorophenyl)isoxazole-3-carboxylate ***(3b)***

White solid (61 % yield). ^{1}H NMR (400 MHz, $CDCl_3$): δ 7.75 (dd, J = 8.4, 2H), 7.47 (dd, J = 8.4, 2H), 6.92 (s, 1H), 4.47 (q, J = 7.0, 2H), 1.44 (t, J = 7.0, 3H). MS (ESI): *m/z* calcd for $C_{12}H_{10}ClNO_3$ $[M+H]^+$ 252.67; found, 252.99.

4.1.5. Ethyl 5-(4-(trifluoromethyl)phenyl)isoxazole-3-carboxylate (3c)

White crystalline (60 % yield). ^{1}H NMR (400 MHz, DMSO-d_6): δ 8.18 (d, J = 8.0, 2H), 7.92 (d, J = 8.0, 2H), 7.70 (s, 1H), 4.39 (q, J = 7.11, 2H), 1.33 (t, J = 7.11, 3H). MS (ESI): *m/z* calcd for $C_{13}H_{11}F_3NO_3$ $[M+H]^+$ 286.23; found, 286.26.

4.1.6. Synthetic procedure for alcohol ***4a-c***

To a suspension of $LiAlH_4$ (17.37 mmol) in dry THF (10 mL), a solution of the opportune isoxazole ethyl ester **3a-c** (5.79 mmol) in dry THF (5 mL) was added dropwise at 0 °C. After the addition was complete, the mixture was maintained at room temperature. The reaction progress was monitored by ESI-MS and TLC. After 3 h, the reaction was quenched by adding drops of water. The lithium salts were filtered out, and the liquid phase was concentrated to furnish a residue that was dissolved in AcOEt. The reaction mixture was extracted with AcOEt (3x30 mL) and H_2O (20 mL). The combined organic phases were then washed with brine and subsequently dried over Na_2SO_4. Finally, the solution was concentrated, and the crude appropriately crystallized using a mixture of AcOEt/petroleum ether.

4.1.7. (5-Phenylisoxazol-3-yl)methanol ***(4a)***

White powder (99 % yield). ^{1}H NMR (400 MHz, DMSO-d_6) δ 7.90–7.85 (m, 2H), 7.54–7.49 (m, 3H), 7.00 (s, 1H), 5.54 (t, J = 6.0, 1H), 4.55 (d, J = 5.8, 2H). MS (ESI): *m/z* calcd for $C_{10}H_9NO_2$ $[M+H]^+$ 176.19; found, 176.20.

4.1.8. (5-(4-chlorophenyl)isoxazol-3-yl)methanol ***(4b)***

White solid (85 % yield). ^{1}H NMR (400 MHz, $CDCl_3$): δ 7.73–7.67 (m, 2H), 7.47–7.42 (m, 2H), 6.58 (s, 1H), 4.81 (s, 2H). MS (ESI): *m/z* calcd for $C_{10}H_8ClNO_2$ $[M+H]^+$ 210.64; found, 210.47.

4.1.9. (5-(4-(trifluoromethyl)phenyl)isoxazol-3-yl)methanol ***(4c)***

White powder (90 % yield). ^{1}H NMR (400 MHz, DMSO-d_6): δ 8.10 (d, J = 8.4, 2H), 7.88 (d, J = 8.8, 2H), 7.19 (s, 1H), 6.53 (s, 1H), 5.59 (t, J = 6.0, 1H), 4.55 (d, J = 6.0, 2H). MS (ESI): *m/z* calcd for $C_{11}H_8F_3NO_2$ $[M+H]^+$ 244.19; found, 244.32.

4.1.10. General procedure for the preparation of compounds ***5a-c***

CBr_4 (7.05 mmol) was added to a solution of the alcohol derivative **4a-c** (4.7 mmol) in CH_2Cl_2 (45 mL), and the reaction was cooled to 0 °C. Once the desired temperature was reached, PPh_3 (7.05 mmol), previously dissolved in CH_2Cl_2 (20 mL), was introduced. The mixture was

stirred at room temperature for 12 h. The progress of the reaction was monitored by TLC. The solvent was evaporated and the crude product was purified by flash column chromatography with AcOEt/petroleum ether as eluent mixture.

*4.1.11. 3-(bromomethyl)-5-phenylisoxazole (**5a**)*

Yellow oil (95 % yield). ^{1}H NMR (400 MHz, DMSO-d_6): δ 7.90–7.87 (m, 2H), 7.56–7.53 (m, 3H), 7.21 (s, 1H), 4.86 (s, 2H). MS (ESI): *m/z* calcd for $C_{10}H_8BrNO$ $[M+H]^+$ 237.99; found, 237.89.

*4.1.12. 3-(bromomethyl)-5-(4-chlorophenyl)isoxazole (**5b**)*

White solid (88 % yield). ^{1}H NMR (400 MHz, $CDCl_3$): δ 7.73–7.69 (m, 2H), 7.47–7.43 (m, 2H), 6.61 (s, 1H), 4.47 (s, 2H). MS (ESI): *m/z* calcd for $C_{10}H_7BrClNO$ $[M+H]^+$ 271.95; found, 272.04.

4.1.13. 3-(bromomethyl)-5-(4-(trifluoromethyl)phenyl)isoxazole (5c)

White solid (90 % yield). ^{1}H NMR (400 MHz, DMSO-d_6): δ 8.11 (d, J = 8.1 Hz, 2H), 7.90 (d, J = 8.2 Hz, 2H), 7.35 (s, 1H), 4.72 (s, 2H). MS (ESI): *m/z* calcd for $C_{11}H_7BrF_3NO$ $[M+H]^+$ 305.97; found, 306.07.

*4.1.14. General synthesis of compounds **6a-c***

To a cold suspension of phthalimide (1.85 mmol) in CH_3CN (30 mL) NaH (2.4 mmol) was added. The mixture was stirred at room temperature for 10 min. Subsequently, the appropriate brominated derivative **5a-c** (1.37 mmol) was added to the suspension. The reaction mixture was refluxed for 4 h. Then the solvent was concentrated, followed by vigorous extraction with AcOEt (3x30 mL) and H_2O (50 mL). The product was crystallized with Et_2O and petroleum ether.

*4.1.15. 2-((5-Phenylisoxazol-3-yl)methyl)isoindoline-1,3-dione (**6a**)*

Off-white solid (87 % yield); ^{1}H NMR (400 MHz, DMSO-d_6): δ 7.84–7.77 (m, 1H), 7.64–7.52 (m, 2H), 7.42–7.39 (m, 1H), 7.37–7.27 (m, 1H), 5.01 (s, 1H). MS (ESI): *m/z* calcd for $C_{18}H_{12}N_2O_3$ $[M+H]^+$ 305.31; found, 305.25.

*4.1.16. 2-((5-(4-chlorophenyl)isoxazol-3-yl)methyl)isoindoline-1,3-dione (**6b**)*

White powder (72 % yield). ^{1}H NMR (400 MHz, DMSO-d_6): δ 7.85–7.76 (m, 2H), 7.59–7.52 (m, 4H), 7.43 (d, J = 7.5 Hz, 2H), 7.23 (s, 1H), 5.00 (s, 2H). MS (ESI): *m/z* calcd for $C_{18}H_{11}ClN_2O_3$ $[M+H]^+$ 339.75; found, 339.66.

*4.1.17. 2-((5-(4-(trifluoromethyl)phenyl)isoxazol-3-yl)methyl) isoindoline-1,3-dione (**6c**)*

White solid (83 % yield). ^{1}H NMR (400 MHz, DMSO-d_6): δ 8.05 (d, J = 8.1 Hz, 2H), 7.99–7.71 (m, 6H), 7.23 (s, 1H), 4.91 (s, 2H). MS (ESI): *m/z* calcd for $C_{19}H_{11}F_3N_2O_3$ $[M+H]^+$ 373.31; found, 373.23.

*4.1.18. General procedure for the synthesis of **7a-c***

The derivative **6a-c** (1.48 mmol) was suspended in EtOH (20 mL). Then, NH_2NH_2 (1.78 mmol) was added, and the mixture was refluxed for 2 h. The reaction was monitored by ESI-MS and TLC. The solvent was evaporated, and the residue extracted with AcOEt and 1 % $NaHCO_3$. The combined organic phases were washed with brine, dried with Na_2SO_4, and evaporated to dryness. The residue was crystallized with Et_2O and petroleum ether.

*4.1.19. (5-Phenylisoxazol-3-yl)methanamine (**7a**)*

Yellowish solid (58 % yield). ^{1}H NMR (400 MHz, DMSO-d_6): δ 7.67–7.65 (m, 2H), 7.46–7.35 (m, 3H), 7.28 (s, 1H), 3.91 (s, 2H), 2.22 (s, 2H). MS (ESI): *m/z* calcd for $C_{10}H_{10}N_2O$ $[M+H]^+$ 175.21; found, 175.24.

*4.1.20. (5-(4-chlorophenyl)isoxazol-3-yl)methanamine (**7b**)*

Yellow solid (43 % yield). ^{1}H NMR (400 MHz, DMSO-d_6): δ 7.60 (d, J = 7.5 Hz, 2H), 7.47 (d, J = 7.5 Hz, 2H), 7.21 (s, 1H), 3.91 (s, 2H), 2.22 (s, 2H). MS (ESI): *m/z* calcd for $C_{10}H_9ClN_2O$ $[M+H]^+$ 209.65; found, 209.04.

*4.1.21. (5-(4-(trifluoromethyl)phenyl)isoxazol-3-yl)methanamine (**7c**)*

Dark yellow solid (61 % yield). ^{1}H NMR (400 MHz, CD_3OD): δ 7.96 (d, J = 8.0 Hz, 2H), 7.75 (d, J = 8.0 Hz, 2H), 6.94 (s, 1H), 3.91 (s, 2H). MS (ESI): *m/z* calcd for $C_{11}H_9F_3N_2O$ $[M+H]^+$ 243.21; found, 243.19.

*4.1.22. General procedure for the synthesis of **9d-e, 21a-g, 24***

To a solution of $NaHCO_3$ (3.06 mmol) in H_2O, the appropriate acids L-proline, **20a-g**, **23** (1.23 mmol) were added. Then, the desired sulfonyl chlorides **8d** or **8e** (1.23 mmol) were introduced, and the mixture was stirred at 50 °C for 16 h. The reaction was monitored by TLC. Upon completion, extraction was conducted using 1 M HCl and ethyl acetate. The combined organic phases were washed with brine and dried with anhydrous Na_2SO_4. The compounds were then crystallized.

*4.1.23. ((4-fluorophenyl)sulfonyl)-L-proline (**9d**)*

White solid (92 % yield). ^{1}H NMR (400 MHz, DMSO-d_6): δ 12.73 (s, 1H). 7.97–7.82 (m, 2H), 7.52–7.31 (m, 2H), 4.10 (dd, J = 8.6, 1H), 3.40–3.35 (m, 1H), 3.15 (m, 1H), 2.00–1.72 (m, 3H), 1.65–1.52 (m, 1H). MS (ESI): *m/z* calcd for $C_{11}H_{12}FNO_4S$ $[M+H]^+$ 274.28; found, 274.25.

*4.1.24. ((5-Chlorothiophen-2-yl)sulfonyl)-L-proline (**9e**)*

Off-white solid (78 % yield). ^{1}H NMR (400 MHz, $CDCl_3$): δ 7.45 (d, J = 4.0 Hz, 1H), 6.99 (d, J = 4.0 Hz, 1H), 4.27 (dd, J = 8.2, 3.6 Hz, 1H), 3.65–3.53 (m, 1H), 3.37–3.24 (m, 1H), 2.26–2.12 (m, 1H), 2.13–1.92 (m, 2H), 1.92–1.77 (m, 1H). MS (ESI): *m/z* calcd for $C_9H_{10}ClNO_4S_2$ $[M+H]^+$ 295.98; found, 296.08.

*4.1.25. 3-((4-fluorophenyl)sulfonyl)thiazolidine-4-carboxylic acid (**21a**)*

Colourless oil (57 % yield). ^{1}H NMR (400 MHz, DMSO-d_6): δ 13.22 (s, 1H), 8.14–7.86 (m, 2H), 7.60–7.30 (m, 2H), 4.87 (dd, J = 7.4, 3.7 Hz, 1H), 4.74 (d, J = 10.3 Hz, 1H), 4.34 (d, J = 10.3 Hz, 1H), 3.10 (dd, J = 11.4, 3.7 Hz, 1H), 2.87 (dd, J = 11.4, 7.4 Hz, 1H). MS (ESI): *m/z* calcd for $C_{10}H_{10}FNO_4S_2$ $[M-H]^-$ 290.30; found, 290.27.

*4.1.26. 1-((4-fluorophenyl)sulfonyl)piperidine-2-carboxylic acid (**21b**)*

Colourless oil (38 % yield). ^{1}H NMR (400 MHz, DMSO-d_6): δ 12.91 (bs, 1H), 7.84–7.81 (m, 2H), 7.40–7.36 (m, 2H), 4.54–4.53 (m, 1H), 3.61–3.60 (m, 1H), 3.16–3.13 (m, 1H), 1,96 (m, 1H), 1.54–1.52 (m, 2H), 1.21–1.19 (m, 3H). MS (ESI): *m/z* calcd for $C_{12}H_{14}FNO_4S$ $[M-H]^-$ 286.30; found, 286.05.

*4.1.27. 1-((4-fluorophenyl)sulfonyl)piperidine-3-carboxylic acid (**21c**)*

Pale yellow solid (76 % yield). ^{1}H NMR (400 MHz, DMSO-d_6): δ 7.80–7.77 (m, 2H), 7.26–7.20 (m, 2H), 3.82–3.78 (m, 1H), 3.58–3.55 (m, 1H), 2.69–2.57 (m, 2H), 2.46–2.40 (m, 1H), 2.02–1.99 (m, 1H), 1.84–1.80 (m, 1H), 1.68–1.55 (m, 1H), 1.47–1.43 (m, 1H). MS (ESI): *m/z* calcd for $C_{12}H_{14}FNO_4S$ $[M-H]^-$ 286.30; found, 286.22.

*4.1.28. 1-((4-fluorophenyl)sulfonyl)piperidine-4-carboxylic acid (**21d**)*

White solid (49 % yield). ^{1}H NMR (400 MHz, DMSO-d_6): δ 12.30 (s, 1H), 7.91–7.72 (m, 2H), 7.60–7.39 (m, 2H), 3.49–3.44 (m, 2H), 2.43 (td, J = 11.6, 2.8 Hz, 2H), 2.31–2.24 (m, 1H), 1.89–1.85 (m, 2H), 1.54 (qd, J = 11.0, 3.9 Hz, 2H). MS (ESI): *m/z* calcd for $C_{12}H_{14}FNO_4S$ $[M+H]^+$ 288.31; found, 288.32.

*4.1.29. 1-((4-fluorophenyl)sulfonyl)indoline-2-carboxylic acid (**21e**)*

White solid (57 % yield). ^{1}H NMR (400 MHz, DMSO-d_6): δ 7.94–7.00 (m, 8H), 4.96 (dd. J = 4.4 Hz, 1H), 3.06 (d, J = 4.8 Hz, 1H), 3.01 (d, J = 4.0 Hz, 1H). MS (ESI): *m/z* calcd for $C_{15}H_{12}FNO_4S$ $[M-H]^-$ 320.32; found, 320.48.

*4.1.30. 1-((4-fluorophenyl)sulfonyl)-1H-indole-3-carboxylic acid (**21f**)*

Off-white solid (15 % yield). ^{1}H NMR (400 MHz, DMSO-d_6): δ 12.98 (s, 1H), 8.38 (s, 1H), 8.30–8.23 (m, 2H), 8.09–8.04 (m, 1H), 8.01–7.95

(m, 1H), 7.52–7.45 (m, 2H), 7.44–7.36 (m, 2H). MS (ESI): *m/z* calcd for $C_{15}H_{10}FNO_4S$ [M − H]$^-$ 318.30; found, 318.18.

4.1.31. 2-((4-fluorophenyl)sulfonyl)-1,2,3,4-tetrahydroisoquinoline-3-carboxylic acid (21g)

White solid (37 % yield). ^{1}H NMR (400 MHz, DMSO-d_6): δ 12.85 (bs, 1H), 7.97–7.85 (m, 2H), 7.45–7.33 (m, 2H), 7.19–7.08 (m, 4H), 4.84 (dd, J = 6.3, 3.3 Hz, 1H), 4.52 (d, J = 15.9 Hz, 2H), 3.13–3.01 (m, 2H). MS (ESI): *m/z* calcd for $C_{16}H_{14}FNO_4S$ [M − H]$^-$ 334.34; found, 334.45.

4.1.32. 4-(tert-butoxycarbonyl)-1-((4-fluorophenyl)sulfonyl)piperazine-2-carboxylic acid (24)

White viscous solid (55 % yield). ^{1}H NMR (400 MHz, DMSO-d_6): δ 12.93 (bs, 1H), 7.86–7.80 (m, 2H), 7.45–7.39 (m, 2H), 4.44–4.35 (m, 1H), 4.28–4.22 (m, 1H), 3.87 (m, 1H), 3.57–3.54 (m, 1H), 3.25–3.22 (m, 1H), 3.16–3.06 (m, 1H), 2.70–2.61 (m, 1H), 1.30 (s, 9H). MS (ESI): *m/z* calcd for $C_{16}H_{21}FN_2O_6S$ [M-Boc]$^+$ 289.30, [M-tBu]$^+$ 333.31; found, 289.32–333.17.

4.1.33. Synthesis of compounds 10–13, 22a-g, 25–26

To a solution of acid **9d-e, 21a-g** or **24** (1.0 mmol) in DMF (5 mL), HATU (1.20 mmol) and DIPEA (1.20 mmol) were added at 0 °C. The mixture was stirred for 5 min, then a solution of the appropriate amine **6a-c** (1.20 mmol) in DMF (5 mL) was added at the same temperature. The reaction was allowed to stir at room temperature, and its progress was monitored by ESI-MS and TLC. Upon completion, the DMF was removed, and the crude product was extracted using ethyl acetate and 10 % aqueous citric acid, 5 % aqueous $NaHCO_3$ and brine. The desired products were purified by column chromatography and/or preparative HPLC.

4.1.34. (S)-1-((4-fluorophenyl)sulfonyl)-N-((5-phenylisoxazol-3-yl)methyl)pyrrolidine-2-carboxamide (10)

Pale yellow solid (48 % yield). ^{1}H NMR (400 MHz, DMSO-d_6): δ 8.70 (t, J = 5.9 Hz, 1H), 7.99–7.88 (m, 2H), 7.80 (dd, J = 8.0, 1.5 Hz, 2H), 7.55–7.41 (m, 5H), 6.83 (s, 1H), 4.46–4.29 (m, 2H), 4.08–4.05 (m, 1H), 3.46–3.42 (m, 1H), 3.22–3.10 (m, 1H), 1.88–1.69 (m, 3H), 1.58–1.45 (m, 1H). ^{13}C NMR (101 MHz, DMSO-d_6): δ 172.05, 163.56, 130.98, 130.88, 129.76, 125.91, 117.16, 116.94, 99.99, 62.01, 49.60, 34.96, 31.24, 24.61. HRMS (LC-MS Base Peak FullMS esi +): *m/z* calcd for $C_{21}H_{20}FN_3O_4S$ [M+H]$^+$ 430.1231; found, 430.1222; error: −2.1645. T_R = 19.45.

4.1.35. (S)–N-((5-(4-chlorophenyl)isoxazol-3-yl)methyl)-1-((4-fluorophenyl)sulfonyl)pyrrolidine-2-carboxamide (11)

Off-white solid (66 % yield). ^{1}H NMR (400 MHz, DMSO-d_6): δ 8.69 (t, J = 5.9 Hz, 1H), 7.95–7.90 (m, 2H), 7.89–7.76 (m, 2H), 7.67–7.53 (m, 2H), 7.53–7.37 (m, 2H), 6.87 (s, 1H), 4.45–4.28 (m, 2H), 4.06 (dd, J = 8.1, 3.7 Hz, 1H), 3.47–3.42 (m, 1H), 3.19–3.13 (m, 1H), 1.84–1.71 (m, 3H), 1.55–1.50 (m, 1H). ^{13}C NMR (101 MHz, DMSO-d_6): δ 172.04, 168.23, 166.36, 163.54, 135.47, 133.56, 130.97, 130.87, 129.87, 127.73, 117.15, 116.93, 100.55, 62.00, 49.59, 34.95, 31.23, 24.60. HRMS (LC-MS Base Peak Full MS esi +): *m/z* calcd for $C_{21}H_{19}ClFN_3O_4S$ [M+H]$^+$ 464.0841; found, 464.0830; error: −2.4974. T_R = 21.74.

4.1.36. (S)-1-((4-fluorophenyl)sulfonyl)-N-((5-(4-(trifluoromethyl)phenyl)isoxazol-3-yl)methyl)pyrrolidine-2-carboxamide (12)

White solid (63 % yield). ^{1}H NMR (400 MHz, $CDCl_3$): δ 7.93–7.99 (m, 4H), 7.71 (dd, J = 8.2 Hz, 2H), 7.40 (bt, 1H), 7.30–7.21 (m, 2H), 6.72 (s, 1H), 4.68–4.60 (m, 2H), 4.16–4.10 (m, 1H), 3.67–3.54 (m, 1H), 3.23–3.12 (m, 1H), 2.31–2.10 (m, 1H), 1.92–1.66 (m, 3H). ^{13}C NMR (101 MHz, $CDCl_3$): δ 171.53, 168.84, 166.96, 164.41, 161.99, 131.62, 130.65, 130.56, 126.13, 126.05, 116.91, 116.69, 100.34, 62.62, 50.00, 35.55, 30.40, 24.46. HRMS (LC-MS Base Peak FullMS esi +): *m/z* calcd for $C_{22}H_{19}F_4N_3O_4S$ [M+H]$^+$ 498.1105; found, 498.1096; error: −1.8389. T_R = 22.52.

4.1.37. (S)-1-((5-chlorothiophen-2-yl)sulfonyl)-N-((5-(4-(trifluoromethyl)phenyl)isoxazol-3-yl)methyl)pyrrolidine-2-carboxamide (13)

White solid (76 % yield). ^{1}H NMR (400 MHz, DMSO-d_6): 8.78 (bt, 1H), 8.05 (dd, J = 8.2 Hz, 2H) 7.91 (dd, J = 8.6 Hz, 2H), 7.69 (d, J = 4.2 Hz, 1H), 7.38 (d, J = 4.2 Hz, 1H), 7.01 (s, 1H), 4.44–4.37 (m, 2H), 4.09 (t, J = 6.2 Hz, 1H), 3.62–3.43 (m, 1H), 3.26–3.19 (m, 1H), 2.01–1.79 (m, 3H), 1.63–1.46 (m, 1H). ^{13}C NMR (101 MHz, DMSO-d_6): δ 171.73, 163.64, 135.94, 135.12, 133.35, 130.78, 130.44, 129.10, 126.75, 101.84, 62.39, 49.92, 34.98, 31.32, 24.64. HRMS (LC-MS Base Peak FullMS esi +): *m/z* calcd for $C_{20}H_{17}ClF_3N_3O_4S_2$ [M+H]$^+$ 520.0374; found, 520.0351; error: −4.3958. T_R = 23.28.

4.1.38. 3-((4-fluorophenyl)sulfonyl)-N-((5-(4-(trifluoromethyl)phenyl)isoxazol-3-yl)methyl)thiazolidine-4-carboxamide (22a)

White solid (21 % yield). δ ^{1}H NMR (400 MHz, DMSO-d_6): δ 8.88 (t, J = 5.9 Hz, 1H), 8.14–7.98 (m, 4H), 7.91 (d, J = 8.3 Hz, 2H), 7.57–7.38 (m, 2H), 7.04 (s, 1H), 4.84 (d, J = 10.8 Hz, 1H), 4.71 (dd, J = 7.2, 4.7 Hz, 1H), 4.48–4.43 (m, 3H), 3.12 (dd, J = 11.5, 4.7 Hz, 1H), 2.81 (dd, J = 11.5, 7.3 Hz, 1H). ^{13}C NMR (101 MHz, DMSO-d_6): δ 169.05, 167.24, 163.66, 162.87, 133.09, 130.90, 130.18, 129.87, 126.19, 116.69, 116.46, 101.31, 64.44, 51.80, 34.67, 34.17. HRMS (LC-MS Base Peak FullMS esi +): *m/z* calcd for $C_{21}H_{17}F_4N_3O_4S_2$ [M+H]$^+$ 516.0669; found, 516.0664; error: −0.9689. T_R = 22.07.

4.1.39. 1-((4-fluorophenyl)sulfonyl)-N-((5-(4-(trifluoromethyl)phenyl)isoxazol-3-yl)methyl)piperidine-2-carboxamide (22b)

White solid (21 % yield). ^{1}H NMR (400 MHz, $CDCl_3$): δ 8.01–7.84 (m, 3H), 7.74 (d, J = 8.3 Hz, 2H), 7.27–7.20 (m, 2H), 6.64 (s, 1H), 4.71–4.66 (m, 1H), 4.62–4.54 (m, 2H), 3.94 (d, J = 14.4 Hz, 1H), 3.19–3.11 (m, 1H), 2.35–2.28 (m, 1H), 1.62–1.45 (m, 2H), 1.44–1.32 (m, 1H), 1.25–1.07 (m, 2H); ^{13}C NMR (101 MHz, $CDCl_3$): δ 170.23, 169.02, 166.64, 164.09, 161.80, 136.17, 129.96, 129.86, 126.21, 116.92, 116.69, 100.25, 56.42, 43.84, 35.86, 24.29, 23.42, 19.95. HRMS (LC-MS Base Peak FullMS esi +): *m/z* calcd for $C_{23}H_{21}F_4N_3O_4S$ [M+H]$^+$ 512.1262; found, 512.1257; error: −0.9763. T_R = 23.60.

4.1.40. 1-((4-fluorophenyl)sulfonyl)-N-((5-(4-(trifluoromethyl)phenyl)isoxazol-3-yl)methyl)piperidine-3-carboxamide (22c)

White solid (58 % yield). ^{1}H NMR (400 MHz, $CDCl_3$): δ 7.94–7.87 (m, 2H), 7.84–7.71 (m, 3H), 7.26–7.22 (m, 2H), 6.64 (s, 1H), 6.50–6.47 (m, 1H), 4.68–4.59 (m, 2H), 3.65 (dd, J = 11.8, 3.4 Hz, 1H), 3.52–3.49 (m, 1H), 2.79 (dd, J = 11.7, 9.4 Hz, 2H), 1.88–1.82 (m, 2H), 1.76–1.65 (m, 4H); ^{13}C NMR (101 MHz, $CDCl_3$): δ 172.91, 166.68, 161.71, 131.99, 130.43, 130.34, 126.24, 126.15, 116.71, 116.48, 100.36, 48.10, 46.43, 42.54, 35.62, 27.12, 23.81. HRMS (LC-MS Base Peak FullMS esi +): *m/z* calcd for $C_{23}H_{21}F_4N_3O_4S$ [M+H]$^+$ 512.1262; found, 512.1249; error: −2.4720. T_R = 22.68.

4.1.41. 1-((4-fluorophenyl)sulfonyl)-N-((5-(4-(trifluoromethyl)phenyl)isoxazol-3-yl)methyl)piperidine-4-carboxamide (22d)

White solid (66 % yield). ^{1}H NMR (400 MHz, DMSO-d_6): δ 8.44 (t, J = 5.8 Hz, 1H), 8.08 (d, J = 8.1 Hz, 2H), 7.88 (t, J = 7.4 Hz, 2H), 7.86–7.78 (m, 2H), 7.56–7.40 (m, 2H), 7.02 (s, 1H), 4.34 (d, J = 5.8 Hz, 2H), 3.62–3.59 (m, 2H), 2.34 (td, J = 11.7, 2.5 Hz, 2H), 2.23–2.16 (m, 1H), 1.84–1.80 (m, 2H), 1.70–1.52 (m, 2H). ^{13}C NMR (101 MHz, DMSO-d_6): δ 173.64, 167.24, 165.68, 163.17, 163.10, 131.91, 130.38, 130.29, 126.23, 126.09, 126.05, 116.57, 116.34, 101.31, 45.14, 34.09, 27.45. HRMS (LC-MS Base Peak FullMS esi +): *m/z* calcd for $C_{23}H_{21}F_4N_3O_4S$ [M+H]$^+$ 512.1262; found, 512.1248; error: −2.6673. T_R = 21.98.

4.1.42. 1-((4-fluorophenyl)sulfonyl)-N-((5-(4-(trifluoromethyl)phenyl)isoxazol-3-yl)methyl)indoline-2-carboxamide (22e)

White solid (20 % yield). ^{1}H NMR (400 MHz, $CDCl_3$): δ 7.87 (d, J = 8.1 Hz, 2H), 7.76–7.72 (m, 3H), 7.70–7.62 (m, 2H), 7.49 (t, J = 5.9 Hz,

1H), 7.30–7.28 (m, 1H), 7.19–7.05 (m, 4H), 6.61 (s, 1H), 4.75–4.68 (m, 2H), 4.56–4.50 (m, 1H), 3.35–3.30 (m, 1H), 2.93–2.90 (m, 1H). ^{13}C NMR (101 MHz, $CDCl_3$): δ 170.82, 161.79, 140.23, 131.95, 131.69, 130.34, 130.17, 130.07, 128.25, 126.41, 126.03, 125.99, 125.37, 118.10, 116.76, 116.54, 100.29, 63.77, 35.62, 32.23. HRMS (LC-MS Base Peak FullMS esi +): *m/z* calcd for $C_{26}H_{19}F_4N_3O_4S$ $[M+H]^+$ 546.1105; found, 546.1086; error: −3.6916. T_R = 22.76.

4.1.43. 1-((4-fluorophenyl)sulfonyl)-N-((5-(4-(trifluoromethyl)phenyl) isoxazol-3-yl)methyl)-1H-indole-3-carboxamide (22f)

White solid (28 % yield). ^{1}H NMR (400 MHz, DMSO-d_6): δ 9.10 (t, J = 5.8 Hz, 1H), 8.59 (s, 1H), 8.17 (dd, J = 7.1, 0.8 Hz, 1H), 8.15–8.06 (m, 4H), 7.93 (d, J = 8.2 Hz, 1H), 7.88 (d, J = 8.2 Hz, 2H), 7.51–7.43 (m, 2H), 7.41–7.31 (m, 2H), 7.20 (s, 1H), 4.58 (d, J = 5.8 Hz, 2H). ^{13}C NMR (101 MHz, DMSO-d_6): δ 167.75, 167.39, 163.10, 162.68, 133.76, 132.75, 130.30, 130.20, 128.39, 128.22, 126.29, 126.09, 125.41, 124.21, 122.17, 117.54, 117.31, 116.16, 112.80, 101.75, 34.27. HRMS (LC-MS Base Peak FullMS esi +): *m/z* calcd for $C_{26}H_{17}F_4N_3O_4S$ $[M+H]^+$ 544.0949; found, 544.0940; error: −1.5916. T_R = 25.03.

4.1.44. 2-((4-fluorophenyl)sulfonyl)-N-((5-(4-(trifluoromethyl)phenyl) isoxazol-3-yl)methyl)-1,2,3,4-tetrahydroisoquinoline-3-carboxamide (22g)

White solid (13 % yield). ^{1}H NMR (400 MHz, DMSO-d_6): δ 8.76 (t, J = 5.9 Hz, 1H), 8.01–7.79 (m, 6H), 7.38–7.23 (m, 2H), 7.18–7.01 (m, 4H), 6.57 (s, 1H), 4.64–4.51 (m, 3H), 4.34–4.21 (m, 2H), 3.01 (dd, J = 15.9, 4.7 Hz, 1H), 2.84 (dd, J = 15.8, 6.4 Hz, 1H). ^{13}C NMR (101 MHz, DMSO-d_6): δ 170.80, 167.62, 163.55, 134.82, 132.86, 132.50, 130.79, 130.69, 128.37, 127.33, 126.71, 126.56, 116.84, 116.62, 101.52, 55.39, 45.67, 34.93, 31.39. HRMS (LC-MS Base Peak FullMS esi +): *m/z* calcd for $C_{27}H_{21}F_4N_3O_4S$ $[M+H]^+$ 560.1262; found, 560.1246; error: −2.7958. T_R = 24.01.

4.1.45. tert-Butyl-4-((4-fluorophenyl)sulfonyl)-3-(((5-(4-(trifluoromethyl)phenyl)isoxazol-3-yl)methyl)carbamoyl)piperazine-1-carboxylate (25)

White solid (31 % yield). ^{1}H NMR (400 MHz, DMSO-d_6): δ 8.84–8.80 (m, 1H), 8.07 (d, J = 8.2 Hz, 2H), 7.89–7.81 (m, 2H), 7.80–7.77 (m, 2H), 7.48–7.25 (m, 2H), 7.02 (s, 1H), 4.41–4.36 (m, 1H), 4.33–4.10 (m, 3H), 3.91–3.82 (bs, 1H), 3.56 (bs, 2H), 3.12–3.07 (m, 1H), 2.90–2.71 (m, 1H), 1.24 (s, 9H); ^{13}C NMR (101 MHz, DMSO-d_6): δ 168.66, 167.29, 165.62, 163.11, 153.14, 134.71, 131.46, 130.24, 130.02, 129.92, 126.20, 125.11, 123.29, 122.40, 116.25, 116.03, 101.52, 53.68, 45.78, 44.56, 41.68, 34.17, 27.64. HRMS (LC-MS Base Peak FullMS esi +): *m/z* calcd for $C_{27}H_{28}F_4N_4O_6S$ $[M+Na]^+$ 635.1557; found, 635.1537; error: −3.2889. T_R = 22.85.

4.1.46. 1-((4-fluorophenyl)sulfonyl)-N-((5-(4-(trifluoromethyl)phenyl) isoxazol-3-yl)methyl)piperazine-2-carboxamide (26)

Off-white solid (37 % yield). ^{1}H NMR (400 MHz, DMSO-d_6): δ 8.96 (t, J = 5.8 Hz, 1H), 8.02 (d, J = 8.1 Hz, 2H), 7.93–7.88 (m, 4H), 7.42–7.32 (m, 2H), 6.97 (s, 1H), 4.72 (d, J = 4.2 Hz, 1H), 4.31 (d, J = 5.8 Hz, 2H), 3.89–3.85 (m, 1H), 3.62–3.53 (m, 3H), 3.20 (d, J = 12.7 Hz, 1H), 2.99 (dd, J = 13.5, 5.0 Hz, 1H), 2.76 (td, J = 12.8, 4.0 Hz, 1H). ^{13}C NMR (101 MHz, DMSO-d_6): δ 168.16, 167.95, 166.47, 163.95, 162.9, 135.06, 130.86, 130.76, 126.78, 117.20, 116.97, 102.03, 51.97, 43.32, 42.03, 35.17. HRMS (LC-MS Base Peak FullMS esi +): *m/z* calcd for $C_{22}H_{20}F_4N_4O_4S$ $[M+H]^+$ 513.1214; found, 513.1199; error: −2.9525. T_R = 16.82.

4.1.47. Synthesis of compounds 14–15

To a solution of the desired isoxazole derivative **12** or **13** (0.28 mmol) in TFA (4 mL), *N*-iodosuccinimide (0.42 mmol) was gradually added at room temperature and maintained under vigorous stirring for 30 min. The reaction was monitored by ESI-MS and TLC. Upon completion, the reaction mixture was evaporated to dryness. The crude product was then extracted with AcOEt and 5 % aqueous $Na_2S_2O_3$, dried with brine and anhydrous Na_2SO_4, and the organic phase was concentrated. For product purification, column chromatography was performed using an eluent mixture of petroleum ether and AcOEt.

4.1.48. (S)-1-((4-fluorophenyl)sulfonyl)-N-((4-iodo-5-(4-(trifluoromethyl)phenyl)isoxazol-3-yl)methyl)pyrrolidine-2-carboxamide (14)

Pale yellow powder (88 % yield). ^{1}H NMR (400 MHz, DMSO-d_6): δ 8.60 (t, J = 5.5 Hz, 1H), 8.21 (d, J = 8.1 Hz, 2H), 8.06–7.86 (m, 4H), 7.57–7.33 (m, 2H), 4.46–4.31 (m, 2H), 4.14 (dd, J = 8.6, 3.2 Hz, 1H), 3.20–3.17 (m, 1H), 1.93–1.78 (m, 2H), 1.74–1.68 (m, 1H), 1.63–1.47 (m, 1H), 1.39–1.24 (m, 1H).^{13}C NMR (101 MHz, DMSO-d_6): δ 171.66, 164.04, 163.84, 161.03, 133.78, 131.16, 130.97, 130.87, 128.27, 127.54, 126.65, 117.12, 116.89, 67.57, 61.87, 49.49, 36.31, 31.17, 24.52. HRMS (LC-MS Base Peak FullMS esi +): *m/z* calcd for $C_{22}H_{18}F_4IN_3O_4S$ $[M+H]^+$ 624.0071; found, 624.0052; error: −3.1394. T_R = 20.50.

4.1.49. (S)-1-((5-chlorothiophen-2-yl)sulfonyl)-N-((4-iodo-5-(4-(trifluoromethyl)phenyl)isoxazol-3-yl)methyl)pyrrolidine-2-carboxamide (15)

Off-white solid (85 % yield). ^{1}H NMR (400 MHz, DMSO-d_6): δ 8.62 (t, J = 5.5, 1H), 8.20 (d, J = 8.2, 2H), 7.97 (d, J = 8.3, 2H), 7.65 (d, J = 4.1, 1H), 7.36 (d, J = 4.2, 1H), 4.41–4.46 (m, 2H), 4.13 (dd, J = 8.3, 3.2 Hz, 1H), 3.54–3.45 (m, 1H), 3.24–3.29 (m, 1H), 1.94–1.85 (m, 2H), 1.84–1.76 (m, 1H), 1.67–1.59 (m, 1H). ^{13}C NMR (101 MHz, DMSO-d_6): δ 174.25, 171.31, 164.20, 164.01, 154.73, 135.85, 135.32, 133.24, 130.83, 129.04, 128.26, 126.61, 67.01, 62.24, 49.83, 36.31, 31.26, 24.53. MS (ESI): *m/z* calcd for $C_{20}H_{16}ClF_3IN_3O_4S_2$ $[M+H]^+$ 646.84; found, 646.25.

4.1.50. General Suzuki procedure for 16–18

The appropriate phenylboronic acid (0.208 mmol) was added to compound **14** or **15** (0.170 mmol) in a toluene/EtOH/H_2O mixture (2:1:1.5). Then, K_2CO_3 (0.60 mmol) was added, followed by the catalyst $Pd(PPh_3)_4$ (0.017 mmol) under an inert atmosphere. The mixture was stirred at 80 °C for 16 h. The reaction was monitored by ESI-MS and TLC. When the reaction was completed, the mixture was extracted with AcOEt/H_2O, the organic phases were washed with brine, and dried with anhydrous Na_2SO_4. The products were purified via column chromatography.

4.1.51. (S)-1-((4-fluorophenyl)sulfonyl)-N-((4-phenyl-5-(4-(trifluoromethyl)phenyl)isoxazol-3-yl)methyl)pyrrolidine-2-carboxamide (16)

White solid (89 % yield). ^{1}H NMR (400 MHz, $CDCl_3$): δ 7.90–7.83 (m, 2H), 7.78–7.74 (m, 1H), 7.65 (d, J = 8.3 Hz, 2H), 7.59 (d, J = 8.4 Hz, 2H), 7.54–7.37 (m, 4H), 7.36–7.30 (m, 2H), 7.25–7.21 (m, 1H), 4.69 (dd, J = 16.3, 6.5 Hz, 1H), 4.41 (dd, J = 16.3, 4.6 Hz, 1H), 4.10 (dd, J = 8.8, 2.9 Hz, 1H), 3.55–3.50 (m, 1H), 3.24–3.04 (m, 1H), 2.11–2.06 (m, 1H), 1.82–1.67 (m, 1H), 1.67–1.53 (m, 2H). ^{13}C NMR (101 MHz, $CDCl_3$): δ 171.66, 164.36, 163.79, 160.15, 133.54, 130.64, 130.55, 129.59, 129.52, 128.95, 127.96, 127.09, 125.75, 116.85, 116.62, 62.38, 49.91, 35.39, 30.29, 24.30. HRMS (LC-MS Base Peak FullMS esi +): *m/z* calcd for $C_{28}H_{23}F_4N_3O_4S$ $[M+H]^+$ 574.1418; found, 574.1392; error: −4.5564. T_R = 24.64.

4.1.52. (S)–N-((4,5-bis(4-(trifluoromethyl)phenyl)isoxazol-3-yl)methyl)-1-((4-fluorophenyl)sulfonyl)pyrrolidine-2-carboxamide (17)

White solid (49 % yield). ^{1}H NMR (400 MHz, $CDCl_3$): δ 7.85 (dd, J = 8.6, 5.0 Hz, 2H), 7.74 (d, J = 8.1 Hz, 2H), 7.65–7.60 (s, 4H), 7.50 (d, J = 8.0 Hz, 2H), 7.31 (bt, 1H), 7.31–7.23 (m, 2H), 4.68 (dd, J = 16.2, 6.2 Hz, 1H), 4.45 (dd, J = 16.2, 4.7 Hz, 1H), 4.01 (d, J = 8.4 Hz, 1H), 3.52–3.48 (m, 1H), 3.15–3.09 (m, 1H), 2.14–2.02 (m, 1H), 1.66–1.54 (m, 3H). ^{13}C NMR (101 MHz, $CDCl_3$): δ 170.95, 166.91, 164.45, 160.00, 132.72, 132.21, 131.88, 131.72, 131.55, 131.16, 130.84, 130.59, 130.50,

130.17, 127.29, 126.42, 126.39, 125.95, 125.92, 125.15, 124.90, 122.44, 122.19, 116.86, 116.63, 115.25, 62.41, 49.91, 35.12, 30.04, 24.29. HRMS (LC-MS Base Peak FullMS esi +): *m/z* calcd for $C_{29}H_{22}F_7N_3O_4S$ $[M+H]^+$ 642.1292; found, 642.1262; error: −1.8747. $T_R = 25.56$.

*4.1.53. (S)–N-((4,5-bis(4-(trifluoromethyl)phenyl)isoxazol-3-yl)methyl)-1-((5-chlorothiophen-2-yl)sulfonyl)pyrrolidine-2-carboxamide (**18**)*

White solid (73 % yield). ^{1}H NMR (400 MHz, $CDCl_3$): δ 7.76–7.69 (m, 2H), 7.65–7.58 (m, 4H), 7.51–7.47 (m, 2H), 7.42–7.39 (m, 1H), 7.31 (t, $J = 5.5$ Hz, 1H), 7.01 (d, $J = 4.0$ Hz, 1H), 4.71–4.64 (m, 1H), 4.52–4.40 (m, 1H), 4.05–4.02 (m, 1H), 3.59–3.51 (m, 1H), 3.23–3.15 (m, 1H), 2.20–2.09 (m, 1H), 1.78–1.62 (m, 3H). ^{13}C NMR (101 MHz, $CDCl_3$): δ 170.91, 164.46, 159.92, 138.48, 133.08, 132.84, 132.65, 130.16, 127.27, 126.40, 125.94, 115.26, 62.72, 50.09, 35.13, 30.03, 29.67, 24.34. HRMS (LC-MS Base Peak FullMS esi +): *m/z* calcd for $C_{27}H_{20}ClF_6N_3O_4S_2$ $[M+H]^+$ 664.0561; found, 664.0532; error: −4.3234. $T_R = 26.53$.

*4.1.54. Sonogashira coupling for the synthesis of **19***

To an anhydrous solution of $PdCl_2(PPh_3)_2$ (0.00224 mmol), CuI (0.00448 mmol), and Et_3N (0.168 mmol) in THF (0.5 mL), phenylacetylene (0.124 mmol) and compound **15** (0.112 mmol) were added at room temperature. The reaction mixture was then heated to 50 °C maintaining an argon atmosphere. After being stirred at this temperature for 12h, the mixture was extracted with ethyl acetate and water. The organic phase was dried with brine and Na_2SO_4, and then evaporated under vacuum. The crude residue was purified via column chromatography using an ethyl acetate and petroleum ether eluent mixture.

*4.1.55. (S)-1-((4-fluorophenyl)sulfonyl)-N-((4-(phenylethynyl)-5-(4-(trifluoromethyl)phenyl)isoxazol-3-yl)methyl)pyrrolidine-2-carboxamide (**19**)*

White solid (42 % yield). ^{1}H NMR (400 MHz, $CDCl_3$): δ 8.31 (d, $J = 8.2$ Hz, 2H), 7.84 (dd, $J = 8.8$, 5.0 Hz, 2H), 7.79 (d, $J = 8.3$ Hz, 2H), 7.61–7.58 (m, 2H), 7.50 (t, $J = 6.0$ Hz 1H), 7.45–7.38 (m, 3H), 7.21 (t, $J = 8.5$ Hz, 2H), 4.94 (dd, $J = 16.3$, 6.8 Hz, 1H), 4.64 (dd, $J = 16.2$, 4.9 Hz, 1H), 4.15 (dd, $J = 8.6$, 2.8 Hz, 1H), 3.58–3.54 (m, 1H), 3.17–3.11 (m, 1H), 2.24–2.14 (m, 2H), 1.90–1.71 (m, 1H), 1.70–1.51 (m, 2H). ^{13}C NMR (101 MHz, $CDCl_3$): δ 171.35, 162.34, 161.98, 131.69, 130.63, 130.54, 129.30, 128.61, 126.51, 125.99, 116.82, 116.60, 62.53, 50.02, 35.20, 30.27, 24.33. HRMS (LC-MS Base Peak FullMS esi +): *m/z* calcd for $C_{30}H_{23}F_4N_3O_4S$ $[M+H]^+$ 598.1418; found, 598.1407; error: −1.8658. $T_R = 26.25$.

4.2. Molecular modeling

TRPA1 protein was retrieved from PDB protein data bank (PDB code: 6WJ5) and subjected to preliminary adjustment for the docking calculations through the protein preparation wizard within Maestro [34]. The hydrogen atoms were added and minimized, the solvent molecules were removed, and the appropriate protonation and tautomeric state of the protein side-chains were calculated at physiological pH. This structure was used for the docking calculations employing the AD4-GPU docking software [26]. Using the AutoDockTools Python scripts, TRPA1 structure was converted in the AutoDock PDBQT format, where, compared to a standard PDB file, Gasteiger charges are added to the atoms and the torsional freedoms of the various bonds are described. Then, the receptor grid maps were calculated with the AutoGrid4 software, mapping the receptor interaction energies using every AutoDock atom type as a probe and the docking grid box was centered on the binding site on the co-crystal structure (XYZ size of the box: 60 60 60 with a spacing of 0.375 Å). The compounds were docked employing standard settings and 200 Lamarkian Genetic Algorithm (LGA) runs. The docking results were subsequently grouped based on the root-mean-square deviation (RMSD) criterion, whereby solutions differing by less than 2.0 Å were considered part of the same cluster. The ranking of these clusters was determined based on the calculated free energy of binding (ΔG_{AD4}). Visualization of the results was carried out using the UCSF Chimera X software [35]. The electrostatic potentials (ESPs) was calculated employing Jaguar standard settings e visualized using UCSF Chimera software [36].

4.3. Cell lines

Human alveolar type II epithelium–like adherent cell line (A549) (CCL-185, American Type Culture Collection, RRID: CVCL_A549) was cultured in RPMI 1640 containing heat-inactivated fetal bovine serum (FBS, 10 %), L-glutamine (2 mM), penicillin (100 U/ml), and streptomycin (10 mg/ml) and HEPES (1 mM). Human embryonic kidney cells (HEK293) stably transfected with cDNA for human TRPA1 (hTRPA1-HEK293) were grown in Dulbecco's Modified Eagle Medium (DMEM) supplemented with FBS (10 %) L-glutamine (2 mM), penicillin (100 U/ml), and streptomycin (10 mg/ml), sodium pyruvate (1 mM) and G418 (1 mg/ml). All cells were maintained in an atmosphere of 95 % air and 5 % CO_2 at 37 °C.

4.4. Calcium imaging

If not otherwise indicated, the reagents were obtained from Merck Life Science SRL. A549 cells were plated on poly-L-lysine–coated (8.3 μM) 35-mm glass coverslips (Thermo Fisher Scientific, Waltham, MA) and maintained at 37 °C in 5 % CO_2 and 95 % O_2 for 24 h before calcium imaging. On the day of experiments, cells were loaded (40 min) with Fura-2 AM-ester (5 μM) added to the buffer solution (37 °C) containing (in mM): 2 calcium chloride, 5.4 potassium chloride, 0.4 magnesium sulphate, 135 NaCl, 10 D-glucose, 10 4-(2-hydroxyethyl)-1-piperazine ethane sulfonic acid, and BSA (0.1 %) at pH 7.4. Cells were stimulated with benzyl isothiocyanate (BITC) (10 μM), after being incubated (10 min) with A967079 (1 nM-100 μM), compound **10** (1 μM), compound **11** (3 nM-10μM), compound **12** (1 nM-10 μM), compound **13** (1 nM-10 μM), compound **14** (1 μM), compound **16** (1 μM), compound **17** (3 nM-30 μM), compound **18** (1 μM), compound **19** (1 μM), compound **22a** (1 μM), compound **22b** (1 μM), compound **22c** (1 μM), compound **22d** (1 μM), compound **22e** (1 μM), compound **22f** (1 μM), compound **22g** (1 μM), compound **25** (1 μM), compound **26** (1 μM) or Veh (0.001 % DMSO). Results were expressed as the percentage of inhibition of response induced by BITC (10 μM). The increase in ratio 340/380 over baseline was normalized to the maximum effect induced by ionomycin (5 μM) added at the end of each experiment.

4.5. Animals

Male mice C57BL/6J (Charles River, RRID: IMSR_JAX:000664) were used (25–30 g, 6–8 weeks old). The group size of n = 8 mice for behavioral experiments was determined by sample size estimation using G Power [37] to detect the size effect in a *post-hoc* test with type 1 and 2 error rates of 5 % and 20 %, respectively. Allocation concealment of mice into the vehicle(s) or treatment groups was performed using a randomization procedure [38]. The assessors were blinded to the allocation to treatment groups. None of the animals were excluded from the study. Mice were housed in a temperature- and humidity-controlled *vivarium* (12 h dark/light cycle, free access to food and water, 5 animals per cage). At least 1 h before behavioral experiments, mice were acclimatized to the experimental room and behavior was evaluated between 9:00 a.m. and 5:00 p.m. Behavioral studies followed Animal Research: Reporting of *In Vivo* Experiments (ARRIVE) guidelines [39]. Animal experiments and sample collections were carried out according to the European Union (EU) guidelines for animal care procedures and Italian legislation (DLgs 26/2014) application of the EU Directive 2010/63/EU. All animal studies were approved by the Animal Ethics Committee of the University of Florence and the Italian Ministry of Health (permits no. #1194/2015-PR).

4.6. Treatment protocols

Mice received intraplantar (i.pl., 10 μl/site or 20 μl/site) injection of allyl isothiocyanate (AITC 10 nmol) or its vehicle (1 % dimethyl sulfoxide, DMSO, in 0.9 % NaCl); Formalin 0.5 % (20 μl); A967079 (1, 3, 10, 30,100, 300 nmol), compound 12 (1, 3, 10, 30,100, 300 nmol), and compound 13 (1, 3, 10, 30,100, 300 nmol) or their vehicle (2 % DMSO, 2 % Tween 80 in 0.9 % NaCl). In the formalin-induced pain model the 80 % inhibitory concentration (ID_{80}) of compound 12 and 13 was tested (50 nmol/10 μl, i.pl.). Antagonists were administered (i.pl.) 30 min before the stimuli (i.pl.).

4.7. Behavioral assays

Acute nociception. Immediately after i.pl. injection, mice were placed inside a plexiglass chamber, and acute nociception response was assessed for 10 min by measuring the time (sec) that the animal spent in lifting, licking, shaking the injected paw.

Formalin test. Mice were placed in a plexiglass cylinder formalin (0.5 % in 0.9 % NaCl) was injected into the plantar surface of the hind paw and bottom-up recorded for 60 min. The total time spent by the mouse lifting, licking, and flinching the paw was considered as nociceptive pain readout. Phases were defined as follows: Phase I (0–9 min), Phase II (10–60 min).

4.8. Statistical analysis

The results are expressed as the mean ± SEM or confidence interval (CI). For multiple comparisons, a one-way ANOVA followed by a post-hoc Bonferroni's test was used. Statistical analyses were performed on raw data using GraphPad Prism 8 (GraphPad Software Inc.). P-values less than 0.05 ($P < 0.05$) were considered significant. IC_{50}, ID_{50} and ID_{80} values were determined from non-linear regression models using Graph Pad Prism 8. The statistical tests used and sample size for each analysis are shown in the Fig. legends.

CRediT authorship contribution statement

Valentina Albanese: Methodology, Investigation. **Matilde Marini:** Methodology, Investigation. **Martina Tesi:** Methodology, Investigation. **Lorenzo Landini:** Methodology, Investigation. **Elisa Bellantoni:** Methodology, Investigation. **Sandro Cosconati:** Writing – review & editing, Writing – original draft, Supervision, Conceptualization. **Michele Roggia:** Methodology, Investigation. **Lorenzo Tagliazucchi:** Methodology, Formal analysis, Data curation. **Lorenzo Gnudi:** Methodology, Investigation. **Valentina Puscio:** Methodology, Investigation. **Chiara Sturaro:** Methodology, Investigation. **Chiara Ruzza:** Writing – review & editing, Supervision. **Remo Guerrini:** Writing – review & editing. **Pierangelo Geppetti:** Writing – review & editing. **Romina Nassini:** Writing – review & editing, Writing – original draft, Supervision, Conceptualization. **Delia Preti:** Writing – review & editing, Writing – original draft, Supervision, Project administration, Conceptualization. **Francesco De Logu:** Writing – review & editing, Writing – original draft, Supervision, Conceptualization. **Salvatore Pacifico:** Writing – review & editing, Writing – original draft, Supervision, Conceptualization.

Declaration of competing interest

The authors declare that they have no known competing financial interests or personal relationships that could have appeared to influence the work reported in this paper.

Acknowledgments

D.P. was supported by Project funded under the National Recovery and Resilience Plan (NRRP), Mission 04 Component 2 Investment 1.5–NextGenerationEU (Call for tender n. 3277 dated December 30, 2021 Award Number: 0001052 dated June 23, 2022). D.P., V.A., R.G., S. P. were supported by local funds from the University of Ferrara. F.D.L., R.N. and P.G. were supported by Fondazione Telethon (Grant no GMR22T1070), Associazione Italiana per la Ricerca sul Cancro (AIRC) under IG 2020 - ID 24503 and European Research Council (ERC) under the European Union's Horizon 2020 research and innovation programme (grant agreement No. 835286).

Appendix A. Supplementary data

Supplementary data to this article can be found online at https://doi.org/10.1016/j.ejmech.2025.117732.

Abbreviations

AITC, allyl isothiocyanate; CI, confidence interval; BITC, benzyl isothiocyanate; DIPEA, diisopropylethylamine; HATU, Hexafluorophosphate Azabenzotriazole Tetramethyl Uronium; TRPA1, transient receptor potential ankyrin 1.

Data availability

Data will be made available on request.

References

[1] J. Li, H. Zhang, Q. Du, J. Gu, J. Wu, Q. Liu, Z. Li, T. Zhang, J. Xu, R. Xie, Research progress on TRPA1 in diseases, J. Membr. Biol. 256 (4–6) (2023) 301–316.
[2] C.E. Paulsen, J.P. Armache, Y. Gao, Y. Cheng, D. Julius, Structure of the TRPA1 ion channel suggests regulatory mechanisms, Nature 520 (7548) (2015) 511–517.
[3] A.P. Koivisto, T. Voets, M.J. Iadarola, A. Szallasi, Targeting TRP channels for pain relief: a review of current evidence from bench to bedside, Curr. Opin. Pharmacol. 75 (2024) 102447.
[4] D. Souza Monteiro de Araujo, R. Nassini, P. Geppetti, F. De Logu, TRPA1 as a therapeutic target for nociceptive pain, Expert Opin. Ther. Targets 24 (10) (2020) 997–1008.
[5] K. Talavera, J.B. Startek, J. Alvarez-Collazo, B. Boonen, Y.A. Alpizar, A. Sanchez, R. Naert, B. Nilius, Mammalian transient receptor potential TRPA1 channels: from structure to disease, Physiol. Rev. 100 (2) (2020) 725–803.
[6] F. De Logu, R. Nassini, S. Materazzi, M. Carvalho Gonçalves, D. Nosi, D. Rossi Degl'Innocenti, I.M. Marone, J. Ferreira, S. Li Puma, S. Benemei, G. Trevisan, D. Souza Monteiro de Araújo, R. Patacchini, N.W. Bunnett, P. Geppetti, Schwann cell TRPA1 mediates neuroinflammation that sustains macrophage-dependent neuropathic pain in mice, Nat. Commun. 8 (1) (2017) 1887.
[7] S.R. Ali, M. Jordan, P. Nagarajan, M. Amit, Nerve density and neuronal biomarkers in cancer, Cancers 14 (19) (2022) 4817.
[8] L. Landini, M. Marini, D. Souza Monteiro de Araujo, A. Romitelli, M. Montini, V. Albanese, M. Titiz, A. Innocenti, F. Bianchini, P. Geppetti, R. Nassini, F. De Logu, Schwann cell insulin-like growth factor receptor type-1 mediates metastatic bone cancer pain in mice, Brain Behav. Immun. 110 (2023) 348–364.
[9] F. De Logu, R. Nassini, A. Hegron, L. Landini, D.D. Jensen, R. Latorre, J. Ding, M. Marini, D. Souza Monteiro de Araujo, P. Ramírez-Garcia, M. Whittaker, J. Retamal, M. Titiz, A. Innocenti, T.P. Davis, N. Veldhuis, B.L. Schmidt, N. W. Bunnett, P. Geppetti, Schwann cell endosome CGRP signals elicit periorbital mechanical allodynia in mice, Nat. Commun. 13 (1) (2022) 646.
[10] D.M. Bautista, S.E. Jordt, T. Nikai, P.R. Tsuruda, A.J. Read, J. Poblete, E. N. Yamoah, A.I. Basbaum, D. Julius, TRPA1 mediates the inflammatory actions of environmental irritants and proalgesic agents, Cell 124 (6) (2006) 1269–1282.
[11] P.G. Baraldi, D. Preti, S. Materazzi, P. Geppetti, Transient receptor potential ankyrin 1 (TRPA1) channel as emerging target for novel analgesics and anti-inflammatory agents, J. Med. Chem. 53 (14) (2010) 5085–5107.
[12] A. Hinman, H.H. Chuang, D.M. Bautista, D. Julius, TRP channel activation by reversible covalent modification, Proc. Natl. Acad. Sci. U. S. A 103 (51) (2006) 19564–19568.
[13] J. Zhao, J.V. Lin King, C.E. Paulsen, Y. Cheng, D. Julius, Irritant-evoked activation and calcium modulation of the TRPA1 receptor, Nature 585 (7823) (2020) 141–145.
[14] Z. Hu, Y. Zhang, W. Yu, J. Li, J. Yao, J. Zhang, J. Wang, C. Wang, Transient receptor potential ankyrin 1 (TRPA1) modulators: recent update and future perspective, Eur. J. Med. Chem. 257 (2023) 115392.
[15] D. Preti, G. Saponaro, A. Szallasi, Transient receptor potential ankyrin 1 (TRPA1) antagonists, Pharm Pat Anal 4 (2) (2015) 75–94.
[16] R.M. Vitale, L. de Petrocellis, P. Amodeo, An updated patent review of TRPA1 antagonists (2020 - present), Expert Opin. Ther. Pat. 34 (5) (2024) 315–332.

[17] A. Balestrini, V. Joseph, M. Dourado, R.M. Reese, S.D. Shields, L. Rougé, D. D. Bravo, T. Chernov-Rogan, C.D. Austin, H. Chen, L. Wang, E. Villemure, D.G. M. Shore, V.A. Verma, B. Hu, Y. Chen, L. Leong, C. Bjornson, K. Hötzel, A. Gogineni, L. Riol-Blanco, A TRPA1 inhibitor suppresses neurogenic inflammation and airway contraction for asthma treatment, J. Exp. Med. 218 (4) (2021) e20201637.
[18] D. Souza Monteiro de Araújo, F. De Logu, C. Adembri, S. Rizzo, M.N. Janal, L. Landini, A. Magi, G. Mattei, N. Cini, P. Pandolfo, P. Geppetti, R. Nassini, K.D. C. Calaza, TRPA1 mediates damage of the retina induced by ischemia and reperfusion in mice, Cell Death Dis. 11 (8) (2020) 633.
[19] A. Paumier, S. Boisseau, M. Jacquier-Sarlin, K. Pernet-Gallay, A. Buisson, M. Albrieux, Astrocyte-neuron interplay is critical for alzheimer's disease pathogenesis and is rescued by TRPA1 channel blockade, Brain: J. Neurol. 145 (1) (2022) 388–405.
[20] S. Gao, K.K. Kaudimba, S. Guo, S. Zhang, T. Liu, P. Chen, R. Wang, Transient receptor potential ankyrin Type-1 channels as a potential target for the treatment of cardiovascular diseases, Front. Physiol. 11 (2020) 836.
[21] J.A. Terrett, H. Chen, D.G. Shore, E. Villemure, R. Larouche-Gauthier, M. Déry, F. Beaumier, L. Constantineau-Forget, C. Grand-Maître, L. Lépissier, S. Ciblat, C. Sturino, Y. Chen, B. Hu, A. Lu, Y. Wang, A.P. Cridland, S.I. Ward, D.H. Hackos, R.M. Reese, M. Volgraf, Tetrahydrofuran-based transient receptor potential ankyrin 1 (TRPA1) antagonists: ligand-based discovery, activity in a rodent asthma model, and Mechanism-of-Action via cryogenic electron microscopy, J. Med. Chem. 64 (7) (2021) 3843–3869.
[22] D.J. Berthelot, H.J.M. Gijsen, M. Zaja, J. Rech, A. Lebsack, B. Branstetter, W. Xiao, J.G. Breitenbucher, Heterocyclic amides as modulators of TRPA1, U.S. Patent 8 (2013), 614,201, Dec 24.
[23] R. Nassini, P. Pedretti, N. Moretto, C. Fusi, C. Carnini, F. Facchinetti, A.R. Viscomi, A.R. Pisano, S. Stokesberry, C. Brunmark, N. Svitacheva, L. McGarvey, R. Patacchini, A.B. Damholt, P. Geppetti, S. Materazzi, Transient receptor potential ankyrin 1 channel localized to non-neuronal airway cells promotes non-neurogenic inflammation, PLoS One 7 (8) (2012) e42454.
[24] J. Chen, S.K. Joshi, S. DiDomenico, R.J. Perner, J.P. Mikusa, D.M. Gauvin, J. A. Segreti, P. Han, X.F. Zhang, W. Niforatos, B.R. Bianchi, S.J. Baker, C. Zhong, G. H. Simler, H.A. McDonald, R.G. Schmidt, S.P. McGaraughty, K.L. Chu, C. R. Faltynek, M.E. Kort, P.R. Kym, Selective blockade of TRPA1 channel attenuates pathological pain without altering noxious cold sensation or body temperature regulation, Pain 152 (5) (2011) 1165–1172.
[25] W.K. Hagmann, The many roles for fluorine in medicinal chemistry, J. Med. Chem. 51 (15) (2008) 4359–4369.
[26] D. Santos-Martins, L. Solis-Vasquez, A.F. Tillack, M.F. Sanner, A. Koch, S. Forli, Accelerating AutoDock4 with GPUs and gradient-based local search, J. Chem. Theor. Comput. 17 (2) (2021) 1060–1073.
[27] C.E. Paulsen, J.P. Armache, Y. Gao, Y. Cheng, D. Julius, Structure of the TRPA1 ion channel suggests regulatory mechanisms, Nature 525 (7570) (2015) 552.
[28] G. Klement, L. Eisele, D. Malinowsky, A. Nolting, M. Svensson, G. Terp, D. Weigelt, M. Dabrowski, Characterization of a ligand binding site in the human transient receptor potential ankyrin 1 pore, Biophys. J. 104 (4) (2013) 798–806.
[29] S.E. Wheeler, Understanding substituent effects in noncovalent interactions involving aromatic rings, Accounts Chem. Res. 46 (4) (2013) 1029–1038.
[30] A.D. Bochevarov, E. Harder, T.F. Hughes, J.R. Greenwood, D.A. Braden, D. M. Philipp, D. Rinaldo, M.D. Halls, J. Zhang, R. A. Jaguar Friesner, A high-performance quantum chemistry software program with strengths in life and materials sciences, Int. J. Quant. Chem. 113 (2013) 2110–2142.
[31] C.R. McNamara, J. Mandel-Brehm, D.M. Bautista, J. Siemens, K.L. Deranian, M. Zhao, N.J. Hayward, J.A. Chong, D. Julius, M.M. Moran, C.M. Fanger, TRPA1 mediates formalin-induced pain, Proc. Natl. Acad. Sci. U. S. A 104 (33) (2007) 13525–13530.
[32] S.M. Jain, R. Balamurugan, M. Tandon, N. Mozaffarian, G. Gudi, Y. Salhi, R. Holland, R. Freeman, R. Baron, Randomized, double-blind, placebo-controlled trial of ISC 17536, an oral inhibitor of transient receptor potential ankyrin 1, in patients with painful diabetic peripheral neuropathy: impact of preserved small nerve fiber function, Pain 163 (6) (2022) e738–e747.
[33] M.M. Mellado Lagarde, D. Wilbraham, R.F. Martins, H.S. Zhao, K. Jackson, K. W. Johnson, K.L. Knopp, D. Di Benedetto, L.M. Broad, Clinical proof-of-concept Results with a Novel TRPA1 Antagonist (LY3526318) in 3 Chronic Pain States, in: Pain, Advance online publication, 2024, https://doi.org/10.1097/j.pain.0000000000003487.
[34] G.M. Sastry, M. Adzhigirey, T. Day, R. Annabhimoju, W. Sherman, Protein and ligand preparation: parameters, protocols, and influence on virtual screening enrichments, J. Comput. Aided Mol. Des. 27 (3) (2013) 221–234.
[35] E.C. Meng, T.D. Goddard, E.F. Pettersen, G.S. Couch, Z.J. Pearson, J.H. Morris, T. E. Ferrin, UCSF ChimeraX: tools for structure building and analysis, Protein Sci.: a publication of the Protein Society 32 (11) (2023) e4792.
[36] E.F. Pettersen, T.D. Goddard, C.C. Huang, G.S. Couch, D.M. Greenblatt, E.C. Meng, T.E. Ferrin, UCSF Chimera–a visualization system for exploratory research and analysis, J. Comput. Chem. 25 (13) (2004) 1605–1612.
[37] F. Faul, E. Erdfelder, A. Buchner, A.G. Lang, Statistical power analyses using g*Power 3.1: tests for correlation and regression analyses, Behav. Res. Methods 41 (4) (2009) 1149–1160.
[38] Research randomized. http://www.randomizer.org/. (Accessed 28 January 2025).
[39] J.C. McGrath, E. Lilley, Implementing guidelines on reporting research using animals (ARRIVE etc.): new requirements for publication in BJP, Br. J. Pharmacol. 172 (13) (2015) 3189–3193.